Biogeosciences, 12, 2227–2245, 2015
www.biogeosciences.net/12/2227/2015/
doi:10.5194/bg-12-2227-2015

Biogeosciences
Open Access

Organic-matter quality of deep permafrost carbon – a study from Arctic Siberia

J. Strauss[1,2], L. Schirrmeister[1], K. Mangelsdorf[3], L. Eichhorn[4], S. Wetterich[1], and U. Herzschuh[1]

[1]Alfred Wegener Institute, Helmholtz Centre for Polar and Marine Research, Periglacial Research Unit Potsdam, Telegrafenberg A 43, Potsdam, Germany
[2]Potsdam University, Institute of Earth and Environmental Science, Karl-Liebknecht-Str. 24–25, 14476 Potsdam, Germany
[3]Helmholtz Centre Potsdam, GFZ German Research Centre for Geosciences, Telegrafenberg, 14473 Potsdam, Germany
[4]International Max Planck Research School for Global Biogeochemical Cycles (Max Planck Institute for Biogeochemistry and Friedrich Schiller University), Burgweg 11, 07749 Jena, Germany

Correspondence to: J. Strauss (jens.strauss@awi.de)

Received: 5 August 2014 – Published in Biogeosciences Discuss.: 21 November 2014
Revised: 15 March 2015 – Accepted: 19 March 2015 – Published: 15 April 2015

Abstract. The organic-carbon (OC) pool accumulated in Arctic permafrost (perennially frozen ground) equals the carbon stored in the modern atmosphere. To give an idea of how Yedoma region permafrost could respond under future climatic warming, we conducted a study to quantify the organic-matter quality (here defined as the intrinsic potential to be further transformed, decomposed, and mineralized) of late Pleistocene (Yedoma) and Holocene (thermokarst) deposits on the Buor-Khaya Peninsula, northeast Siberia. The objective of this study was to develop a stratigraphic classified organic-matter quality characterization. For this purpose the degree of organic-matter decomposition was estimated by using a multiproxy approach. We applied sedimentological (grain-size analyses, bulk density, ice content) and geochemical parameters (total OC, stable carbon isotopes (δ^{13}C), total organic carbon : nitrogen (C / N) ratios) as well as lipid biomarkers (*n*-alkanes, *n*-fatty acids, hopanes, triterpenoids, and biomarker indices, i.e., average chain length, carbon preference index (CPI), and higher-plant fatty-acid index (HPFA)). Our results show that the Yedoma and thermokarst organic-matter qualities for further decomposition exhibit no obvious degradation–depth trend. Relatively, the C / N and δ^{13}C values and the HPFA index show a significantly better preservation of the organic matter stored in thermokarst deposits compared to Yedoma deposits. The CPI data suggest less degradation of the organic matter from both deposits, with a higher value for Yedoma organic matter. As the interquartile ranges of the proxies mostly overlap, we interpret this as indicating comparable quality for further decomposition for both kinds of deposits with likely better thermokarst organic-matter quality. Supported by principal component analyses, the sediment parameters and quality proxies of Yedoma and thermokarst deposits could not be unambiguously separated from each other. This revealed that the organic-matter vulnerability is heterogeneous and depends on different decomposition trajectories and the previous decomposition and preservation history. Elucidating this was one of the major new contributions of our multiproxy study. With the addition of biomarker data, it was possible to show that permafrost organic-matter degradation likely occurs via a combination of (uncompleted) degradation cycles or a cascade of degradation steps rather than as a linear function of age or sediment facies. We conclude that the amount of organic matter in the studied sediments is high for mineral soils and of good quality and therefore susceptible to future decomposition. The lack of depth trends shows that permafrost acts like a giant freezer, preserving the constant quality of ancient organic matter. When undecomposed Yedoma organic matter is mobilized via thermokarst processes, the fate of this carbon depends largely on the environmental conditions; the carbon could be preserved in an undecomposed state till refreezing occurs. If modern input has occurred, thermokarst organic matter could be of a better quality for future microbial decomposition than that found in Yedoma deposits.

Published by Copernicus Publications on behalf of the European Geosciences Union.

1 Introduction

During the late Quaternary, the rate of organic-matter decomposition in the Arctic was slower than plant growth, sedimentation, and freezing rates. Thus, a large pool of organic carbon (OC) accumulated in the Arctic and was sequestered deep in the permafrost. Hugelius et al. (2014) estimates an OC storage of 1300 Gt for the circum-Arctic permafrost region with ∼ 850 Gt OC sequestered in permafrost. This is approximately the carbon stored in the modern atmosphere (Dlugokencky and Tans, 2014). During warming and permafrost thawing, this formerly cryo-sequestered OC gradually entered the modern biogeochemical cycle by microbial turnover. By thawing and microbial activity, the permafrost deposits can turn from a carbon sink to a source (Schuur et al., 2009), releasing greenhouse gases such as carbon dioxide and methane to the atmosphere. In addition to the near-surface carbon pool representing the uppermost 3 m below surface, deep OC pools, especially those held in ice-rich permafrost deposits in the Yedoma region, are of great significance for current concerns about the effects of global warming because of rapid permafrost thaw, such as thermokarst and thermoerosion. According to Strauss et al. (2013) and Hugelius et al. (2014), the Yedoma region is defined as the area of potential distribution of late Pleistocene ice-rich and organic-rich silty deposits (Yedoma), covering large areas in Siberia and Alaska. Estimates of OC stored in the Yedoma region amount to 83 ± 12 Gt for late Pleistocene Yedoma deposits (ages shown in Table 1). Due to Holocene warming, subsequent ground ice melt and surface subsidence, thermokarst basins formed and were partly occupied by lakes. Holocene thermokarst deposits (ages shown in Table 1) contain 130 ± 29 Gt organic carbon. In total, the Yedoma region extends to an area of about 1 387 000 km^2, of which about 70 % is already affected by permafrost degradation (thermokarst; Strauss et al., 2013). Kuhry et al. (2009) and Schirrmeister et al. (2011a) showed that Yedoma deposits accumulated at fast rates, implying a short time for the organic matter to decay before it became locked into a perennially frozen state. Therefore, the organic-matter availability for microorganisms is expected to be excellent, resulting in great vulnerability to warming ground conditions (Mu et al., 2014). To elucidate how the Yedoma region permafrost could respond under conditions of future climatic warming, we studied the organic-matter degradation state of Yedoma and its Holocene degradation features (called thermokarst deposits) on the Buor-Khaya Peninsula, eastern Laptev Sea. As mentioned above, Strauss et al. (2013) found that thermokarst deposits contain the quantitatively more important carbon pool, but the unsolved question is this: is the thermokarst organic-matter pool as degradable as the frozen late Pleistocene Yedoma, or has the most labile carbon already been emitted due to thermokarst degradation processes? In both kinds of deposits the OC was incorporated deep (deeper than 3 m) into permafrost (Schirrmeister et al., 2013; Strauss et al., 2013). As shown by models and extrapolation from recent observations, the more southern portions of Yedoma deposits thawed during the last deglaciation, resulting in large emissions of greenhouse gases to the atmosphere (Walter et al., 2007a; Ciais et al., 2012; Walter Anthony et al., 2014). Recent ground warming has been observed in the permafrost zone (Romanovsky et al., 2010), and incubation experiments reveal that permafrost warming is accompanied by a substantial outgassing of greenhouse gases (Lee et al., 2012; Knoblauch et al., 2013; Schädel et al., 2014). As an illustration of the important influence of ground temperature on organic-matter degradation, a higher respiration rate at greater depth close to the permafrost table (Mangelsdorf et al., 2009; Waldrop et al., 2010) was found inside the seasonally thawed active layer and interpreted as a greater lability of the organic matter close to the perennially frozen ground. Focusing on permafrost deposits in the Laptev Sea region, which includes our Buor-Khaya study site, Schirrmeister et al. (2011a) characterize the Yedoma region permafrost organic matter as weakly decomposed.

Biomarkers are used for the paleoenvironmental reconstruction of terrestrial permafrost (Andersson et al., 2011) or the characterization of permafrost organic-matter degradation (Andersson and Meyers, 2012; Vonk et al., 2013; Routh et al., 2014). In our study we estimate molecular markers (*n*-alkanes, *n*-fatty acids, hopanes, and triterpenoids) and use biomarker proxies and indices (absolute lipid concentration, average chain length (ACL), carbon preference index (CPI), hop-17(21)-ene, higher-plant fatty-acid (HPFA) index, and an oleanene ratio) to test whether they are useful mirrors of organic-matter decomposition, i.e., of the organic-matter state of degradation in permafrost deposits. Fairly established methods, both cryolithological (grain-size analyses, bulk density, ice content) and biogeochemical (total organic carbon ($TOC_{wt\,\%}$), stable carbon isotope ratios ($\delta^{13}C$ in TOC), total nitrogen (TN), and $TOC_{wt\,\%}$ / TN (C / N) ratios), are applied to our sample set. Finally, principal components analysis (PCA) highlights the relationships between different organic-matter degradation proxies.

Because the future feedback from the Yedoma region permafrost OC to climate forcing is driven by both (1) the pool size, estimated to be ∼ 211 Gt (Strauss et al., 2013), and (2) the state of degradation of OC stored in the studied deposits, the objective of this study is the development of a stratigraphically differentiated organic-matter quality characterization using sample material representative of widespread Yedoma and thermokarst permafrost. We hypothesize increased organic-matter degradation during thermokarst processes but also increased organic-matter input during climatically favorable Holocene times.

Table 1. Radiocarbon dating on plant macroremains. Calibrations were done by using the Calib 6.0 software and the IntCal09 calibration curve (Stuiver et al., 2010). Depth is given in meters below surface level (m b.s.l.) and height in meters above sea level (m a.s.l.). Age is given as year before present (yr BP). Poz: Poznań Radiocarbon Laboratory, Poland.

Lab. no.	Sample name	Depth (m b.s.l.)	Height (m a.s.l.)	Radiocarbon ages (yr BP)	±	Calibrated ages 2σ (95.4 %) (yr BP)	±	
Poz-42080	Buo-03-A-03	1.3	28.7	4760	40	5519	70	thermokarst deposits
Poz-42072	Buo-01-A-02	0.7	8.7	3665	35	3990	100	
Poz-42073	Buo-01-A-04	1.8	7.6	8140	50	9075	78	
Poz-42086	Buo-05-A-04	0.8	8.7	5990	40	6837	103	
Poz-42087	Buo-05-B-10	3.4	6.1	8000	80	8817	215	
Poz-42088	Buo-05-B-19	6.1	3.4	7940	50	8811	122	
Poz-42090	Buo-05-C-23	7.3	2.2	5280	35	6059	74	
Poz-42091	Buo-05-C-29	9.2	0.3	6710	90	7566	138	
Poz-42074	Buo-02-A-03	0.7	29.3	30 100	300	34 613	596	Yedoma deposits
Poz-42075	Buo-02-B-09	3.5	26.5	34 650	550	39 813	1242	
Poz-42076	Buo-02-B-12	5	25	41 500	1500	45 312	2649	
Poz-42077	Buo-02-D-20	5.5	24.5	45 000	2000	47 614	2386	
Poz-42078	Buo-02-D-23	7	23	43 000	1500	46 830	2678	
Poz-42081	Buo-04-A-02	1.5	17.1	49 000	3000			
Poz-42082	Buo-04-A-08	5	13.6	> 48 000				
Poz-42083	Buo-04-B-10	8.5	9.1	> 55 000				
Poz-42084	Buo-04-C-16	10.5	8	> 49 000				
Poz-42085	Buo-04-C-20	11.7	6.8	> 55 000				

2 Materials and methods

2.1 Study area

The Buor-Khaya Peninsula study site (71°34′ N, 132°12′ E) is located in the northeastern part of Siberia (Fig. 1). The Buor-Khaya Peninsula is framed by the Laptev Sea, a shallow epicontinental part of the Arctic Ocean, and geologically by two rift structures (Drachev et al., 1998). Buor-Khaya is underlain by continuous permafrost with ground temperatures of less than −11 °C (Drozdov et al., 2005). The permafrost thickness is estimated to be between 450 and 650 m (Romanovskii et al., 2004). Stratigraphically, outcrops from two sediment units are distinguished and studied: (1) ice-rich permafrost, called Yedoma deposits, and (2) deposits in permafrost rapid-thaw features, generalized as thermokarst deposits. Three profiles of thermokarst deposits (in a thermokarst basin: Buo-01 and Buo-05; initial thermokarst on top of a Yedoma hill: Buo-03) and two profiles of Yedoma deposits (Buo-02, Buo-04) were studied and sampled. Figure 1 shows an overview of the sampled profiles and their position relative to each other.

2.2 Field work

Field studies were undertaken in summer 2010 at outcrops situated on the western coast of the Buor-Khaya Peninsula. The sediment of the profiles and sub-profiles, exposed at the cliff wall or partly in thermokarst mounds in thaw slumps, was dug with spades and cleaned with hacks. The cryolithology, sediment characteristics, and visible organic matter in the sediments of the sequences chosen were surveyed and described. Moreover, the profiles were photographed and sketched. Sub-profiles were stacked together to create composite profiles. Sampling positions in neighboring sub-profiles were correlated by height estimation using measuring tape. The upper edge of each profile was calibrated with tacheometer measurements (Günther et al., 2012). In the field laboratory, all sample volumes were measured with a balance following Archimedes principle, and the absolute ice content was determined by drying the sample. In total, 91 samples were taken and cooled for transport to laboratories for further analysis. The detailed sampling positions for each profile are shown in Strauss and Schirrmeister (2011).

2.3 Indicators of organic-matter quality for further decomposition

To validate and to extend the sedimentological approach used and to estimate the organic-matter quality for further decomposition, lipid biomarkers were measured in order to estimate the degree of organic-matter degradation. For biomarker studies we used a "fingerprint" approach by focusing on identifiable markers related to the state of organic-matter degradation. Below, the geochemical indicators and biomarkers used are described.

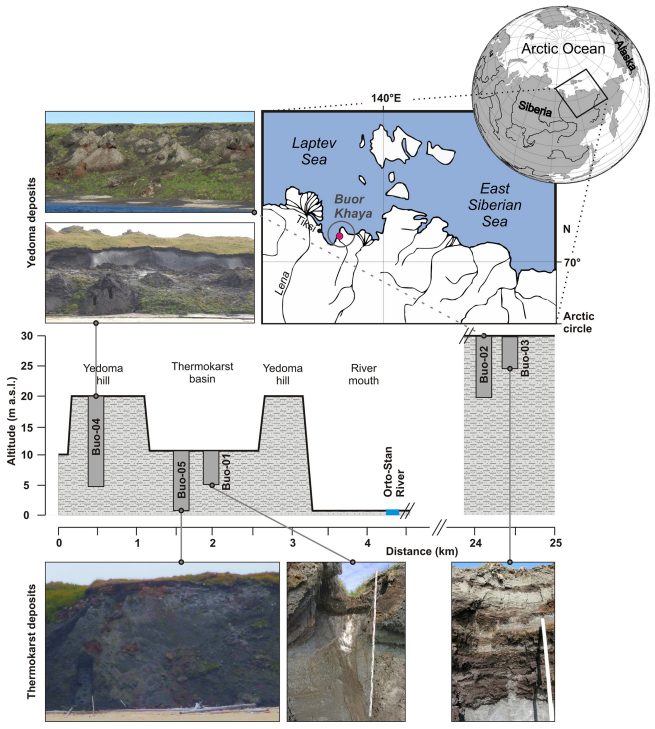

Figure 1. Location of the Buor-Khaya Peninsula and the study area. The square black box in the globe inset indicates the area shown in the map below. The profile diagram and the photographs below it show the profiles and their positions relative to each other. Adapted from Strauss and Schirrmeister (2011); pictures taken by J. Strauss.

2.3.1 Grain-size analyses

Grain sizes were analyzed using a laser particle sizer (LS 200, Beckmann-Coulter) with a measuring range of 0.375 to 1000 µm (Figs. 2, S1 in the Supplement). Grain-size calculations were done following Folk and Ward (1957) using Gradistat v8 (Blott and Pye, 2001). A detailed description of these analytical techniques is given in the Supplement (Sect. S1.1 in the Supplement).

2.3.2 Elemental composition

To determine the total elemental carbon and total nitrogen (TN) content, the samples were measured by a carbon–nitrogen–sulfur analyzer (Vario EL III, Elementar). $TOC_{wt\,\%}$ was measured with a TOC analyzer (Vario Max C, Elementar). The volumetric TOC content ($TOC_{kg\,m^{-3}}$) was calculated according to Strauss et al. (2013). A detailed description of this technique is given in the Supplement (Sect. S1.2).

The TOC / TN (C / N) ratio has been used as a general indicator of the degree of organic-matter decomposition (Stevenson, 1994). Based on the assumption that organic-matter components are degraded selectively, degradation modifies elemental compositions and hence C / N in deposits. Because a decrease in the C / N ratio has been observed in aerated deposits with microbial immobilization of TN (nitrogen stays in the system) accompanied by the remineralization of TOC (Sollins et al., 1984) and CO_2 emission, this ratio is used in the following way: the higher the C / N ratio, the lower the degree of decomposition.

2.3.3 Bulk density and volumetric carbon content

BD (bulk density) was calculated using Eq. (1).

$$\mathrm{BD}\ [10^3\,\mathrm{kg\,m^{-3}}] = \frac{\text{sample dry weight}\ [10^3\,\mathrm{kg}]}{\text{sample volume}\ [\mathrm{m^3}]} \quad (1)$$

Estimating the BD is required in order to convert the measured-weight-based $TOC_{wt\,\%}$ content per sample to a volume-based value. Thus, the $TOC_{kg\,m^{-3}}$ was calculated according to Eq. (2):

$$TOC_{kg\,m^{-3}} = \mathrm{BD}\ [10^3\,\mathrm{kg\,m^{-3}}] \times \frac{TOC_{wt\%}}{100}. \quad (2)$$

2.3.4 Carbon isotope studies

Stable TOC carbon isotopes were determined with a Finnigan MAT Delta-S mass spectrometer combined with a FLASH elemental analyzer and a ConFlo III gas mixing system. A detailed methodology is given in the Supplement (Sect. S1.4). The stable carbon isotopes of OC reflect (1) an initial contribution from different plant species and plant components and (2) subsequent degradation processes (Gundelwein et al., 2007). Assuming constant photosynthetic isotope fractionation in source plants in the region (C_3 plants are ubiquitous in the Arctic; Tieszen, 1973), we use $\delta^{13}C$ ratios as a degradation proxy. According to Heyer et al. (1976), decomposition discriminates against the lighter isotope (^{12}C), resulting in more negative $\delta^{13}C$ ratios. Thus, this proxy is used in the following way: lower (more negative) $\delta^{13}C$ values are connected to less degraded material, while higher (less negative) $\delta^{13}C$ values reflect greater decomposition.

Ages were determined by radiocarbon dating of selected macroscopic plant remains performed at the Poznań Radiocarbon Laboratory, Poland (Goslar et al., 2004). The presented radiocarbon ages are uncalibrated ages; Table 1 includes calibrated ages as well. Radiocarbon ages are given in year before present (yr BP).

2.3.5 Lipid biomarkers

To look more closely at the molecular composition, we used specific lipid biomarkers. Molecular fossils or biomarkers were studied by chromatography methods coupled with mass spectrometers. Characteristic fractions like *n*-alkanes, *n*-fatty acids, sterols, and hopanes were isolated. Because the $TOC_{wt\,\%}$ in the profiles is not equally distributed, we calculated and visualized the biomarker concentration as $\mu g\,gTOC_{wt\,\%}^{-1}$ and $\mu g\,gSediment^{-1}$ ($\mu g\,gSed^{-1}$). For the results, we focus on $\mu g\,gTOC_{wt\,\%}^{-1}$. Every radiocarbon-dated

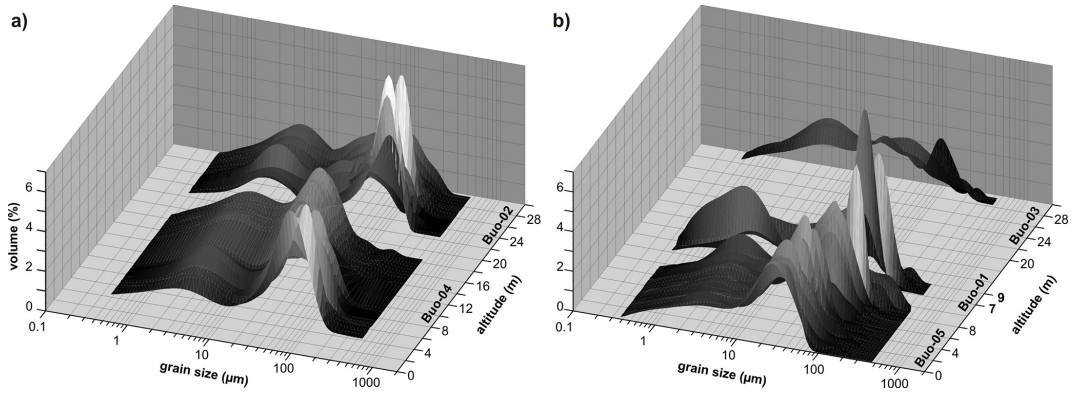

Figure 2. Three-dimensional grain-size distributions of **(a)** Yedoma and **(b)** thermokarst profiles. To avoid an overlap of Buo-05 and Buo-01 in **(b)**, the altitude axis was adapted and does not ascend consistently. A two-dimensional grain-size plot is shown in Fig. S1.

sample and additional samples were used for biomarker analysis. In total 25 biomarker samples were analyzed. Independently of $TOC_{wt\,\%}$, the sample selection for biomarkers was based on their stratigraphic position with the aim of covering the maximum time period.

Extraction and fraction separation

For lipid biomarker analyses, 2–12 g of ground sediment was weighed in an extraction cell with an accelerated solvent extractor (ASE 200, Dionex). Samples were extracted with dichloromethane / methanol (99 : 1). Each sample was held in a static phase for 20 min at 75 °C (after 5 min heating, no preheating) at a pressure of 5 MPa. Afterwards, the dissolved compounds were concentrated with a TurboVap (Zymark) closed-cell concentrator and further dried by evaporating the solvent in a stream of nitrogen gas. After that, internal standards (5α-androstane for the aliphatic fraction, ethylpyrene for the aromatic fraction, 5α-androstan-17-on for nitrogen-, sulfur-, and oxygen- (NSO-) containing compounds and erucic acid for the NSO fatty-acid fraction) were added. The amount of internal standards depended on the $TOC_{wt\,\%}$ content (< 10 wt%: 8 µg; > 10 to ≤ 25 wt%: 20 µg; > 25 wt%: 50 µg). After the removal of the *n*-hexane-insoluble fraction (by the addition of a large excess of *n*-hexane, called "asphaltene" precipitation), the hexane-soluble portion of the extract was separated by medium-pressure liquid chromatography (MPLC; Radke et al., 1980) into fractions of different polarity (aliphatic and aromatic hydrocarbons as well as polar hetero- (NSO) components). Afterwards, the NSO fraction was split into a fatty acids and an alcohol fraction using a KOH-impregnated silica gel column (Schulte et al., 2000).

For this study, the focus was placed on the aliphatic fraction (containing *n*-alkanes and triterpenoid compounds) and the NSO fraction (containing *n*-fatty acids). The fractions were measured by gas chromatography–mass spectrometry (GC-MS). All compounds of interest were identified using the Xcalibur software (Thermo Fisher Scientific).

GC-MS measurement and compound quantification

The *n*-alkanes, *n*-alcohols, hopenes (hop-17(21)-ene), and other triterpenoids (β-amyrin (olean-12-en-3β-ol), olean-12-ene, and olean-13(18)-ene) were measured with a GC-MS system (GC – Trace GC Ultra; MS – DSQ; both Thermo Fisher Scientific). Prior to the measurements, the *n*-fatty acids were methylated with diazomethane and the alcohols were silylated with *N*-methyl-*N*-trimethylsilyltrifluoroacetamide (MSTFA). The GC was equipped with a programmable temperature vaporization (PTV) injector system (starting temperature of 50 °C, heating rate of 10 °C s^{-1} to 300 °C, isothermal holding time of 10 min, operated in splitless mode) and a fused silica capillary column (SGE BPX5, 50 m length, 0.22 mm inner diameter, 0.25 µm film thickness). For the measurements the GC oven was programmed with a starting temperature of 50 °C, a heating rate of 3 °C min^{-1} to 310 °C, and an isothermal holding time of 30 min. Helium with a constant flow rate of 1 mL min^{-1} was used as a carrier gas. For the *n*-fatty-acid fraction a different temperature program (starting temperature of 50 °C, 1 min isotherm, heating rate of 3 °C min^{-1} to 350 °C, isothermal holding time 25 min) was used. For compound identification, the gas chromatograph was linked to a mass spectrometer, which was operated in electron impact ionization mode at 70 eV. The temperature of the ion source was set to 230 °C. Full scan mass spectra were recorded from m/z 50 to 600 Da at a scan rate of 2.5 scans s^{-1}. For the *n*-fatty-acid fraction, the scan rate was m/z 50 to 650 Da.

The quantification of *n*-alkanes, *n*-fatty acids, and β-amyrin was done in the GC-MS total ion current chromatogram by relating the peak area of the target compound to the peak area of an internal standard of known concentration. Other triterpenoids like olean-12-ene, olean-13(18)-ene, and hopene were quantified using the m/z 191 mass trace relative to the peak area of the β, β-diploptene (in the m/z 191 mass trace), the concentration of which was calculated in the to-

tal ion current chromatogram relative to the internal standard (5α-androstane).

2.3.6 Biomarker proxies and indices

Absolute lipid concentration

The absolute lipid concentration is used as a rough estimator of organic-matter quality for degradation in the following way: the higher the concentration, the better the conservation of the lipid and the better the quality of the organic matter.

Carbon preference index

The CPI was introduced by Bray and Evans (1961) as the ratio of odd- to neighboring even-numbered alkanes; this is a measure of the alteration of organic matter. Here we use the improved formula from Marzi et al. (1993). In addition, we also applied the CPI for fatty acids in which even-numbered fatty acids predominate over adjacent odd n-fatty acids (Glombitza et al., 2009).

$$\mathrm{CPI} = \frac{\left(\sum_{i=n}^{m} C_{2i+1}\right) + \left(\sum_{i=n+1}^{m+1} C_{2i+1}\right)}{2 \times \left(\sum_{i=n+1}^{m+1} C_{2i}\right)}, \quad (3)$$

where n is the starting dominating chain length/2, m is the ending dominating chain length/2, i is the index (carbon number), and C is concentration.

The CPI is used as a degradation and alteration proxy by quantifying the odd over even (n-alkanes, Fig. S2) or even over odd (n-fatty acids, Fig. S3) predominance of the carbon chains (Bray and Evans, 1961; Glombitza et al., 2009). A low CPI means mature or degraded organic matter (e.g., CPI of crude oil ~ 1).

Average chain length

As introduced by Poynter (1989), the n-alkane ACL value is the concentration-weighted mean of different carbon chain lengths in a geological sample. For n-alkanes we use the C_{23}–C_{33} interval, for n-fatty acids the C_{20}–C_{34}:

$$\mathrm{ACL} = \frac{\sum i \times C_i}{\sum C_i}, \quad (4)$$

where i is the index (carbon number) and C is concentration.

The ACL is a rough OC source parameter. A schematic showing different chain lengths in different organisms is given in Fig. S4. The higher C_3 land plants are expected to have an ACL of $\sim$ 28–29.

Hop-17(21)-ene

We use hop-17(21)-ene as another marker for low-maturity organic material. The hop-17(21)-ene is produced by bacteria. The assumption here is that during degradation and diagenesis the hop-17(21)-ene will be transformed into saturated hopane (Luo et al., 2012).

Higher-plant fatty-acid index

The ratio of the major even wax alcohols over the sum of major odd wax alkanes plus even alcohols was introduced by Poynter (1989) as the higher-plant alcohol (HPA) index. It is applied as an indicator for chemical degradation of the wax components. Based on this index, but using fatty acids instead of alcohols, we developed the HPFA index. The general assumption for this index is that it reflects the preservation degree of organic matter due to the higher lability of n-fatty acids in relation to n-alkanes.

$$\mathrm{HPFA} = \frac{\sum n\text{-fatty acids } C_{24}, C_{26}, C_{28}}{\sum n\text{-fatty acids } C_{24}, C_{26}, C_{28} + \sum n\text{-alkanes } C_{27}, C_{29}, C_{31}} \quad (5)$$

The HPFA ratio cannot be considered an absolute index of degradation but is an indicator of the relative amounts of the more labile fatty acids that remain in a sample. Since n-alkanes are preserved preferentially compared to n-fatty acids, a decrease in this index indicates increased decomposition (the more degraded, the lower the HPFA index).

Oleanene ratio

β-Amyrin (olean-12-en-3β-ol) is a triterpenoid produced by higher land plants. As a first degradation step, β-amyrin is expected to lose its hydroxy group and will be transformed to olean-12-ene. A second step would be a shift of the double-bond-forming olean-13(18)-ene. Thus, fresh organic material is associated with a lower oleanene ratio, while more degraded organic matter is reflected in a higher ratio. This index is calculated as follows:

$$\text{oleanene ratio } (\%) = \frac{\text{olean-12-ene} + \text{olean-13(18)-ene}}{\beta\text{-amyrin}} \cdot 100. \quad (6)$$

Acetate

Pore water was obtained from each sample by centrifugation in specific pore water tubes. Water extracts were analyzed twice using ion chromatography with conductivity detection (ICS 3000, Dionex). An analytical column (AS 11 HC, 2 × 250 mm, Dionex) was used at a constant 35 °C. The sample was eluted with a KOH solution of varying concentration over time. The initial concentration was 1.4 mM. Between 0 and 6 min, the KOH solution was increased at a constant rate to 1.6 mM. Between 6 and 12 min the solution was increased to 10.0 mM KOH, and a concentration of 15.0 mM KOH was reached at 22 min. After 32 min, 60.0 mM KOH concentration was achieved, maintained for 1 min, and followed by a rapid decrease to 1.4 mM after 33 min, when samples were fixed for 45 min to equilibrate the system. For

the quantification of acetate, standards containing the investigated compound were measured. The standard deviation of the sample and of standard quantification was < 5 %. Because acetate can act as excellent feedstock for microbes (Smith and Mah, 1980; Vieth et al., 2008) and it has been shown that acetate was rapidly consumed in the presence of oxygen and nitrate (Kuesel and Drake, 1995), we use the acetate pore water concentrations in the different deposits as a parameter to assess the quality of the organic matter and to compare the potential of the different deposits for future microbial degradation.

2.4 Statistical methods

2.4.1 Significance testing

For testing the samples concerning their statistical distribution, the Shapiro–Wilk normality test was applied. Because of non-normal distribution, we used the Mann–Whitney–Wilcoxon test for significance testing of Yedoma and thermokarst samples. In order to compare the five different profiles, we used the Kruskal–Wallis rank sum test.

2.4.2 Principal component analysis

Multivariate statistical techniques, such as the PCA used here, allow the analysis of multiple variables in order to investigate connections between the different degradation proxies. Prior to the PCA, concentration data were transformed using a log $(x+1)$ transformation. As the square root transformation is commonly applied to count data, especially if the values are mostly rather small, we decided to use this weaker (compared to logarithm) transformation for the TOC ($_{\mathrm{wt\,\%}}$ and $_{\mathrm{kg\,m^{-3}}}$) data. Both transformations were applied to reduce right skewness and to put the parameters on the same scale. We performed three PCA runs. First, a PCA of the sediment parameters was implemented to infer differences between Yedoma and thermokarst deposits. Second, a PCA of biomarker proxies was performed. For this purpose, other characteristics were added as supplementary variables ($\mathrm{TOC_{wt\,\%}}$, $\mathrm{TOC_{kg\,m^{-3}}}$, C / N, δ^{13}C, grain size, BD, ice content, and depth) without being included in the PCA calculation. These supplementary variables have no influence on the PCA and were plotted afterwards in the PCA biplot. Third, a PCA was conducted on samples of the major odd *n*-alkanes to infer possible changes in the source organisms with the same supplementary variables as described above. Computations were performed using the "vegan" package of R software (Oksanen, 2013).

3 Results

Stratigraphically, there are two types of deposition units at the study site. The first unit is composed of Yedoma deposits. The second unit represents thermokarst deposits resulting from thermal degradation of Yedoma. Grain-size distributions (Figs. 2, S1) and PCA of sediments illustrate that thermokarst deposits are made up of degraded Yedoma sediments. According to Gubin and Veremeeva (2010) and Zanina et al. (2011), the Yedoma deposit soil types are mainly less developed cryopedoliths containing more developed paleocryosol parts (Figs. 3 and 4, labeled and grey shaded areas).

3.1 Organic-matter quality of Yedoma deposits

3.1.1 Sedimentological and biogeochemical proxies

The radiocarbon ages (Table 1, Fig. S5) of the Yedoma deposits range from infinite ages (> 55 000 yr BP) at the very bottom to 30 100 yr BP at the uppermost sampled Yedoma unit. This is comparable to other Yedoma sequences in the region (Schirrmeister et al., 2011b). The mean grain sizes show a decreasing trend in the Buo-04 lower Yedoma profile, from 28 µm at the bottom to 11 µm in the upper part of Buo-04-A. The Buo-02 Yedoma profile shows no trend but exhibits a more heterogeneous mean grain size, including three maxima at 22.5 m a.s.l. (32 µm), 23.7 m a.s.l. (34 µm), and 25.5 m a.s.l. (33 µm). Nevertheless, all Yedoma deposit samples are classified as poorly sorted medium-to-coarse silts with a stable low clay fraction (< 15 %).

The $\mathrm{TOC_{wt\,\%}}$ contents vary from 0.2 wt% at 5 m a.s.l to 24.0 wt% in a peaty paleocryosol horizon at 24 m a.s.l. (Fig. 3). The mean $\mathrm{TOC_{wt\,\%}}$ content is 2.4 wt% (median 0.97 wt%). Calculating the $\mathrm{TOC_{kg\,m^{-3}}}$ according to Strauss et al. (2013), by utilizing the BD (between 0.1 and 1.5 10^3 kg m^{-3}; 10^3 kg m^{-3} = g cm^{-3}) and ice content (without ice wedges; 21 to 90 vol %), the Yedoma sediments contain from 3 to 46 kg C m^{-3} with a mean of 14 kg C m^{-3} (median 9 kg C m^{-3}). The maxima correspond to the peaty horizons with large $\mathrm{TOC_{wt\,\%}}$ contents and a low BD. Within the paleocryosol horizons, located at 6.8, 24.0 to 24.5, 24.8, and 27.8 to 28.9 m a.s.l., maxima in the C / N ratio are observable. The C / N range in these horizons is 8 to 31. In the cryopedolith profile parts, the C / N maximum is reached in the lowermost Buo-04-C sub-profile (17.7 and 16.7). The C / N of the rest of the Yedoma profile falls between 4.1 (at Buo-02-C, 23.7 m a.s.l.) and 14.3 (below the paleocryosol at 23.5 m a.s.l.)

The δ^{13}C of the Yedoma deposits ranges from −29.0 to −24.7 ‰. The minima fit the maxima of the C / N ratio well in the paleocryosol horizons at 6.8, 24.0 to 24.5, 24.8, and 27.8 to 28.9 m a.s.l. The minimum C / N of the Buo-02-C sub-profile corresponds approximately to the δ^{13}C maximum (−25.0 to −24.7 ‰).

3.1.2 Biomarker proxies and indices

A series of long-chain *n*-alkanes that exhibit a strong odd-carbon preference ranging from *n*-C_{21} to *n*-C_{33} are iden-

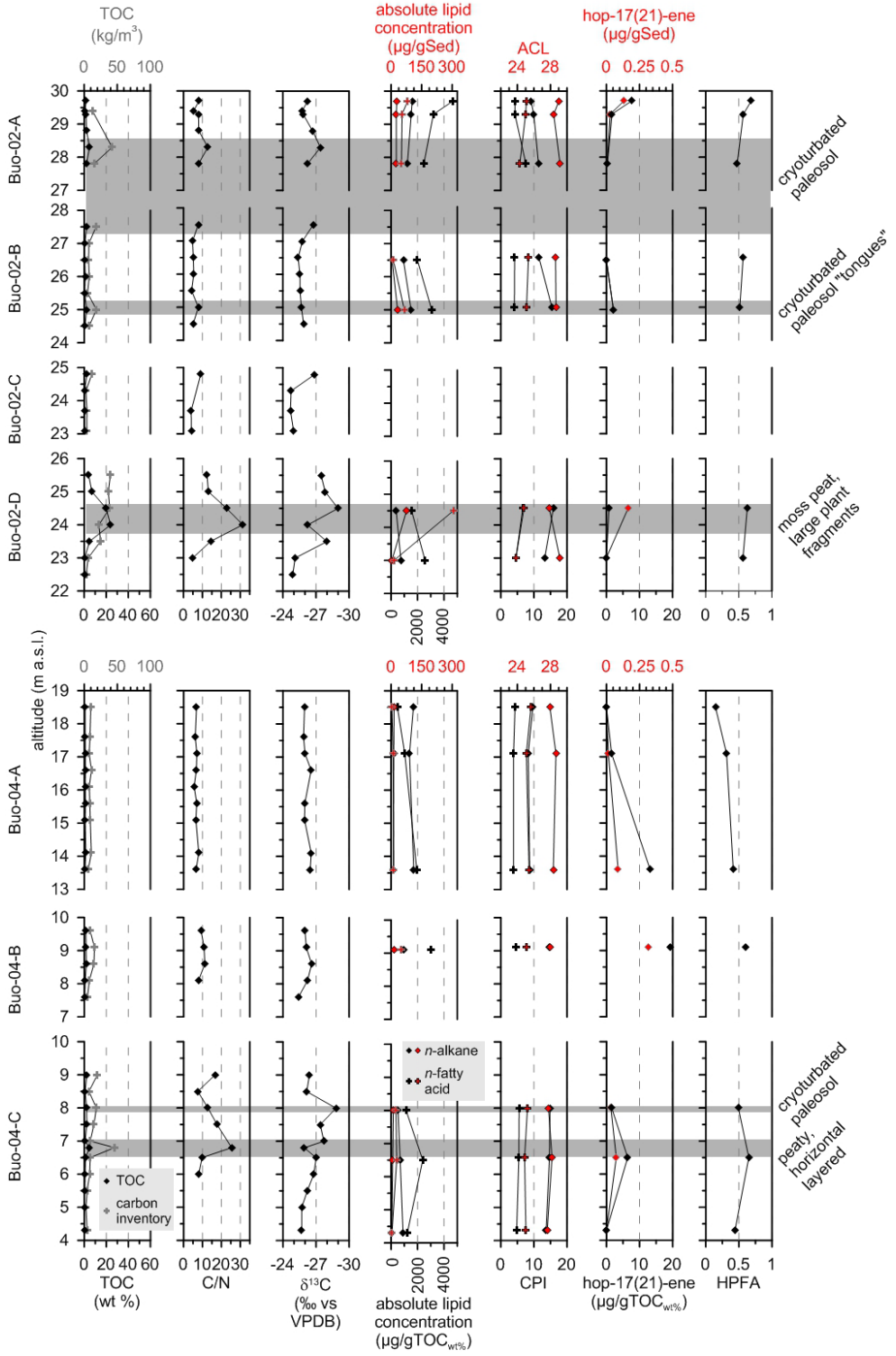

Figure 3. Summary of sedimentological, biogeochemical, and biomarker parameters for the Buo-04 and Buo-02 Yedoma profiles. All diagrams are drawn in such a way as to show more degraded samples on the left and less degraded samples on the right side. Thus, the axis of $\delta^{13}C$ shows descending values. In the text, the paleocryosol parts are reported with altitude measurements from the lowest to the highest sample of each paleocryosol. The grey shaded areas are for visualization, not for exact height estimations of the paleocryosols.

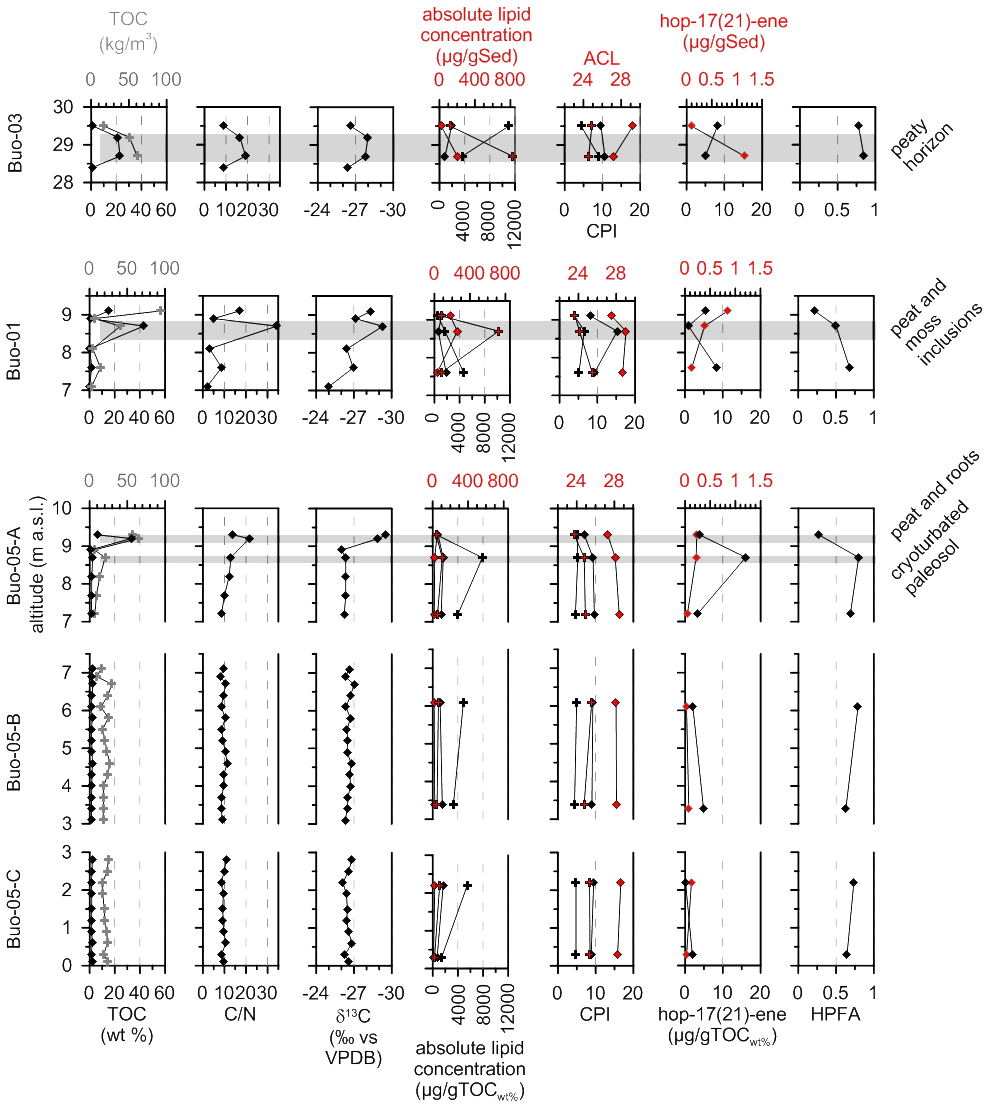

Figure 4. Summary of sedimentological, biogeochemical, and biomarker parameters for the Buo-05, Buo-01, and Buo-03 thermokarst profiles. The *n*-alkane and *n*-fatty-acid symbols are explained in Fig. 3. All diagrams are drawn in such a way as to show more degraded samples on the left and less degraded samples on the right side (descending axis of $\delta^{13}C$ values). In the text, the paleocryosol parts are reported with altitude measurements from the lowest to the highest sample of each paleocryosol. The grey shaded areas are for visualization, not for exact height estimations of the paleocryosols.

tified in all Yedoma samples (Fig. S2). Moreover, the *n*-alkanes show a unimodal distribution maximizing at the C_{27}, C_{29}, or C_{31} *n*−alkane (Fig. S2). The *n*-fatty acids show strong even over odd carbon number predominance and a bimodal distribution ranging from C_{14} to C_{30} (Fig. S3). The maxima are generally located at *n*-C_{16} in the lower carbon number range and at *n*-C_{24} in the higher carbon number range. Total *n*-alkane and *n*-fatty-acid concentrations related to $TOC_{wt\,\%}$ and sediment weight show a homogeneous pattern similar to that of the $TOC_{wt\,\%}$ and C / N values. The *n*-alkane concentration ranges from 3 to 75 µg $gSed^{-1}$ (mean 20 µg $gSed^{-1}$) and from 387 to 1715 µg $TOC^{-1}_{wt\,\%}$ (mean 1132 µg $TOC^{-1}_{wt\,\%}$). The *n*-fatty acids range from 4 to 306 µg $gSed^{-1}$ (mean 51 µg $gSed^{-1}$) and from 475 to 4669 µg TOC^{-1} (mean 2196 µg $TOC^{-1}_{wt\,\%}$).

This Yedoma series shows a distinct preference between even and odd carbon. The mean CPI values of the *n*-alkanes (12.2, ranging from 8.3 to 15.9) are higher than the CPI values of the *n*-fatty acids (4.9, ranging from 3.8 to 7.6). Because *n*-fatty acids are functional compounds (including a functional group, e.g., a carboxyl group), their degradation rates are much higher compared to those of *n*-alkanes (Poynter and Eglinton, 1990). This statement is also based on the assumption of similar sources. The ACL of the *n*-alkanes

and *n*-fatty acids is very stable at around 28.4 (range: 27.6 to 29.2) and 25.0 (range: 23.8 to 25.6), respectively.

Relatively higher hop-17(21)-ene concentrations are used as an indicator for a lower organic-matter degradation state. In the lower Yedoma profile, the hop-17(21)-ene ranges from 0.0 µg $gTOC^{-1}$ in the lowermost and uppermost samples (4.3 and 18.5 m a.s.l.) to the overall maximum of 19.4 µg $gTOC^{-1}$ at the Buor-Khaya site (9.1 m a.s.l.). At Buo-02, the hop-17(21)-ene concentration is lower compared to the other Yedoma profile, with a mean of 1.9 µg $gTOC^{-1}_{wt\%}$ and a maximum of 7.7 µg $gTOC^{-1}_{wt\%}$ in the potentially Holocene-contaminated uppermost sample. The HPFA ratio for the Yedoma samples is very stable around the mean value of 0.50 (median 0.54), with a minimum in 18.5 m a.s.l. (0.15) and a maximum at the uppermost sample (0.69) at 29.7 m a.s.l. For Yedoma, the oleanene ratio is 0.0 (except for a ratio of 10.0 in the uppermost sample). The acetate content of the Yedoma sample is between 0.6 and 57.5 mg L^{-1}, with a mean of 6.7 mg L^{-1} (median 1.2 mg L^{-1}).

3.2 Organic-matter quality of thermokarst deposits

3.2.1 Sedimentological and biogeochemical proxies

The radiocarbon dating shows Holocene ages between 8140 ± 50 and 3665 ± 35 yr BP (Fig. S6, Table 1). The lowermost Buo-05-C profile shows an age inversion for the two samples (0.3 and 2.2 m a.s.l.). The mean grain size at Buo-05 from the bottom to 6.7 m a.s.l. is 13 µm. Above, the mean grain size increases to 19 µm. The Buo-05 clay fraction is stable at a low level (< 15 %). The Buo-01 profile shows a very scattered grain size ranging from 4 to 44 µm mean grain size. For the whole data set, there is a maximum in the clay fraction (35 %) in the peat horizon at 8.7 m a.s.l. Buo-03 shows a slight decrease from 18 to 11 µm. All thermokarst deposits are classified as (very) poorly sorted silts. Similarly to the Yedoma deposits, the BD of the thermokarst deposits is between 0.1 and 1.5 × 10^3 kg m^{-3} and the ice content (without the ice wedges) is 23 to 87 wt% (Fig. 4).

The mean $TOC_{wt\%}$ contents of the thermokarst deposits, 4.7 wt% (median 1.7 wt%), are higher compared to Yedoma deposits, varying between 0.2 and 43.0 wt%. Minimum and maximum $TOC_{wt\%}$ both occur at Buo-01 and exhibit the same scatter as in the grain sizes. $TOC_{kg\,m^{-3}}$ ranges between 2.8 and 93.5 kg C m^{-3} (mean 24, median 19 kg C m^{-3}).

At Buo-05 the C / N ratio is stable at around 9 to 10 (Fig. 4), except for a paleocryosol horizon at 9.2 m a.s.l. that shows a value of 22. At Buo-01, the C / N ratio below the paleocryosol horizon is remarkably low, between 2 and 9, followed by the overall maximum in the peaty horizon with a ratio of 34. The Buo-03 cryopedolith samples show C / N ratios around 10, while the paleocryosol samples exhibit C / N ratios from 16 to 19. The $\delta^{13}C$ values range between −29.5 and −25.0 ‰, with minima corresponding to the C / N maxima at the paleocryosol horizons (anticorrelated to the C / N, Fig. 5a).

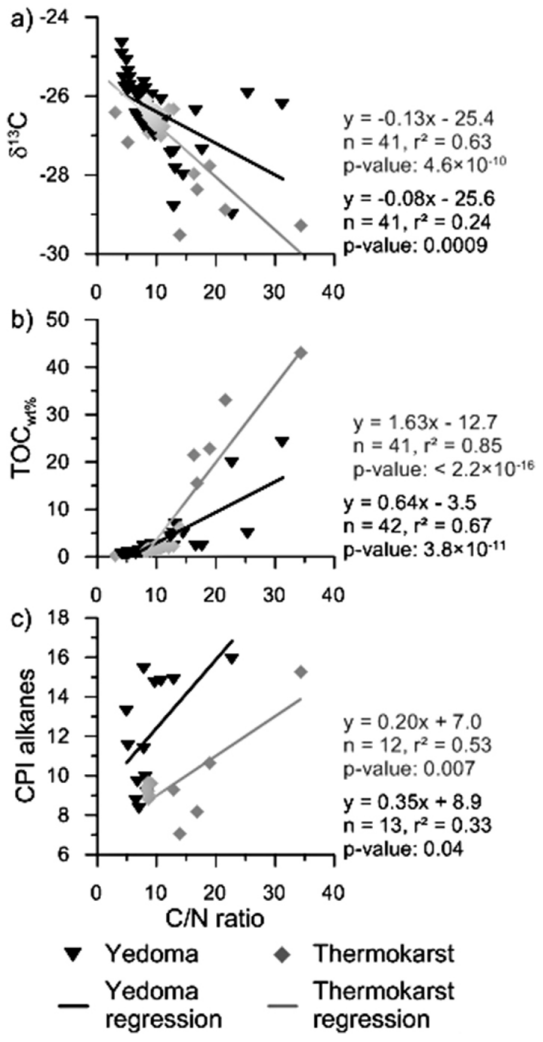

Figure 5. Scatterplots of selected degradation markers. In all three plots, the *x* axis shows the C / N ratio. Yedoma deposits are shown as black triangles, thermokarst deposits as grey diamonds. Regression equations, the r^2, the sample number (*n*), and the *p* value are given to the right of the graph.

3.2.2 Biomarker proxies and indices

The absolute lipid concentration of *n*-alkanes are in the same range but slightly higher compared to the Yedoma profiles. The *n*-alkane average is 1275.7 µg $gTOC^{-1}_{wt\%}$ (median 1260.1 µg $gTOC^{-1}_{wt\%}$), ranging from 599.7 (8.7 m a.s.l.) to 1907.2 µg $gTOC^{-1}_{wt\%}$ (29.5 m a.s.l.). The *n*-fatty-acid average is nearly double that found in the Yedoma samples. On average, 4096.1 µg $gTOC^{-1}_{wt\%}$ (median 3805.7 µg $gTOC^{-1}_{wt\%}$) are stored in the thermokarst deposits of Buor-Khaya, ranging from 554.5 (uppermost Buo-01

sample) to 11013.3 µg $gTOC^{-1}_{wt\%}$ (uppermost Buo-03 sample).

A series of long-chain *n*-alkanes were recognized in all thermokarst samples with a strong odd carbon number preference ranging from *n*-C_{21} to *n*-C_{33}. Nearly all samples show a unimodal distribution of *n*-alkanes maximized at C_{27}, C_{29}, or C_{31} (Fig. S2). Sample Buo-03-A-03 alone does not fit into this scheme because it maximizes at *n*-C_{25}. Compared to Yedoma samples, the short-chain fraction < *n*-C_{27} is more pronounced (Fig. S2). The *n*-fatty acids show a strong even-carbon-number preference and a bimodal distribution between *n*-C_{14} and *n*-C_{30} (Fig. S3), but the *n*-C_{16} is less pronounced than in the Yedoma deposits. An exception to this is found in sample Buo-01-A-02, where the C_{16} monomer reaches the overall maximum of the distribution. Apart from that, the maxima are generally located at the C_{24} *n*-fatty acid.

The *n*-alkane CPI of thermokarst averages 9.6 (median 9.3) and is lower compared to the Yedoma deposits, although the CPI values are in the same range (between 7.0 and 15.3). The CPI of the fatty acids ranges from 4.0 to 9.0 (mean 5.3, median 4.9). The ACL of *n*-alkanes and fatty acids reveal a homogeneous signal between 27.2 and 29.2 (mean 28.3) for *n*-alkanes and 23.6 to 25.6 (mean 24.8) for *n*-fatty acids.

Except for the maximum value of 16.1 µg $gTOC^{-1}_{wt\%}$ at 8.7 m a.s.l., the hop-17(21)-ene concentration at Buo-05 varies between 0.1 and 4.9 µg $gTOC^{-1}_{wt\%}$. Buo-01 paleocryosol values are 0.9 (8.7 m a.s.l.) and 8.4 in the lowermost sample (7.8 m a.s.l.). For Buo-03 the hop-17(21)-ene concentration ranges from 5 up to 8 µg $gTOC^{-1}_{wt\%}$.

The HPFA ratio for the Buo-05 thermokarst samples is high, between 0.6 and 0.8; only the uppermost sample (9.3 m a.s.l.) shows a lower value of 0.2. The Buo-01 profile decreases from 0.7 in the lowest sample to 0.2 at the top. Buo-03 shows high parameter values of 0.8 and 0.9. The oleanene ratio for the thermokarst deposits ranges between 0 (Buo-01) and 13.8 (Buo-03). The overall mean oleanene ratio in thermokarst is 3.7 (median 2.2), which is remarkably higher compared to the Yedoma deposits.

The acetate content of the thermokarst samples is between 0.4 and 109.4 mg L^{-1}, with a mean of 23.5 mg L^{-1} (median 2.8 mg L^{-1}). Large acetate contents are found especially in the middle part of Buo-05, from 3.4 m a.s.l. (74.1 mg L^{-1}) to 6.1 m a.s.l. (109.4 mg L^{-1}), and in the uppermost Buo-03 sample (35.3 mg L^{-1}).

3.3 Statistical methods

3.3.1 Significance testing

Except for the Yedoma CPI, the Yedoma HPFA and the thermokarst hop-17(21)-ene Shapiro–Wilk normality tests reveal a non-normal distribution. Based on this, we chose non-parametric significance testing. This reveals significant differences for TOC, C / N, $\delta^{13}C$, and HPFA on the stratigraphical level (Yedoma vs. thermokarst, Mann–Whitney–Wilcoxon test, Table S1 in the Supplement). On the profile level, we found significant differences for C / N, $\delta^{13}C$, and HPFA by applying the Kruskal–Wallis test (Table S1).

3.3.2 Principal component analyses

The first PCA diagram (Fig. 6a) shows that thermokarst sediments, especially at Buo-05, could not be separated from Yedoma deposits. This diagram, including the first two principal components, explains 79 % (pc1 57 %, pc2 22 %) of the total data set variance. The second PCA diagram (Fig. 6b) illustrates that biomarker quality estimators in Yedoma samples have slightly lower variability because they cluster in an area at pc1 and pc2 > 0, while the thermokarst samples do not cluster. In this diagram 53 % of the data set variance is explained. Moreover, this PCA shows that there is good consistency between the CPI_{alkane} quality estimator and the C / N ratio (Fig. 6b). The PCA of the *n*-alkane chain length (Fig. 6c) shows that the best separating variables for thermokarst are the shorter-chain *n*-alkanes (C_{17}, C_{19}, and C_{21}), contrary to C_{29} for the majority of the Yedoma samples. The pc1 explains 39 and pc2 explains 29 % (total 68 %) of the data set variance.

4 Discussion

The Buor-Khaya Peninsula is a typical Yedoma hill–thermokarst basin landscape of the Yedoma region (Strauss et al., 2013). The Yedoma deposits cover ∼ 15 % of the peninsula (Günther et al., 2013), which is less than the Yedoma region mean of 30 %, but within the overall range of Yedoma deposit coverage (Grosse et al., 2013; Strauss et al., 2013). Thus, the current study of Yedoma and thermokarst deposits is representative of an area covered by similar permafrost deposits of late Pleistocene and Holocene age.

4.1 Sediment facies

The grain-size distribution curves (Figs. 2, S1) indicate a constant deposition environment for the Yedoma sequences. According to Strauss et al. (2012), there have been stable deposition conditions during Yedoma accumulation; this hypothesis is supported by the data presented here. The three thermokarst profiles include three different kinds of thermokarst deposits. Buo-05 is dominated by a lake facies containing valves of two freshwater ostracod taxa: *Cytherissa lacustris* and *Cypria* sp. Moreover, shells have been found in Buo-05 (Strauss and Schirrmeister, 2011). An ice wedge is located next to Buo-01, which points to subaerial conditions, such as a polygon mire. Buo-03 is interpreted as initial thermokarst on top of a Yedoma hill. Thus, the grain-size distributions of Buo-05 and Buo-01 reveal that the thermokarst is granulometrically composed of the same material as Yedoma. The grain-size distributions in Buo-03 paint a different picture. This distribution is likely caused

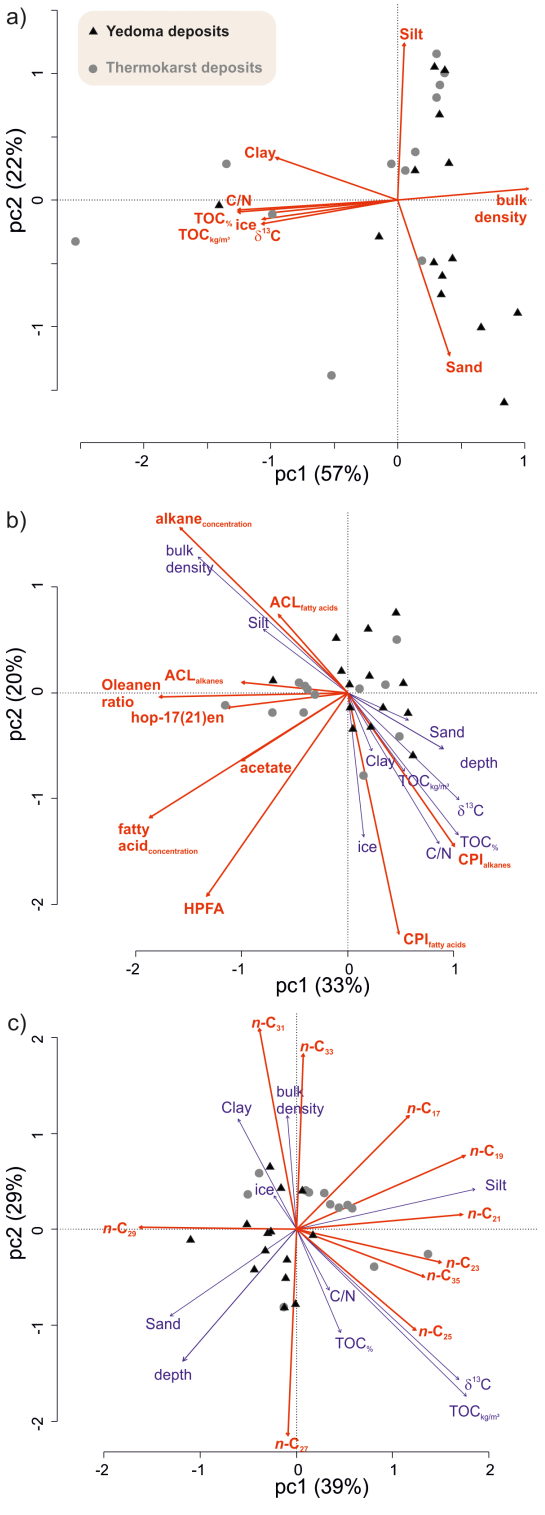

Figure 6. Ordination plots of the principal component analyses (PCA). In diagram **(a)** the sedimentological parameters are plotted. In **(b)** a PCA of biomarker proxies is shown. Supplementary variables (in blue: $TOC_{wt\,\%}$, C / N, $\delta^{13}C$, grain size, BD, ice content) were added without including them in the PCA calculation. In diagram **(c)** the PCA of the major odd *n*-alkanes is visualized using the same supplementary variables as in **(b)**.

by the early state of thermokarst development dominated by peat aggradation. This peat can act like a selective sediment trap influencing the grain-size distributions, e.g., by producing a less distinct coarse-silt–fine-sand peak.

4.2 Organic-matter degradation

The organic-matter proxies of Yedoma deposits are less variable than those of thermokarst deposits (Buo-01 and 03). Except for the paleocryosols, the cryopedolith parts of the Yedoma and the Buo-05 thermokarst profile reveal a rather homogeneous picture (Figs. 3, 4, S5, S6). Constant grain-size distributions, less $TOC_{wt\,\%}$, and smaller absolute lipid concentration scattering reveal that the OC stored in the Yedoma deposits has likely been kept perennially frozen since incorporation. The organic-matter signatures (Figs. 4, S2, and S3) as well as the grain-size distributions (Figs. 2, S1) of thermokarst deposits, especially in Buo-01 and Buo-03, show broader variations. This is caused by a more complex degradation and redeposition history due to reworking. The degradation markers of organic matter found in the paleocryosol parts of all profiles reveal a less degraded state, indicating that the organic matter in these portions is the best preserved.

The mean $TOC_{wt\,\%}$ content for Yedoma deposits is comparable to other sites (Fig. S7) in the Yedoma region (Schirrmeister et al., 2011b, 2013). Intense accumulation and frozen preservation of plant remains ($14\,kgC\,m^{-3}$ for Yedoma and $24\,kgC\,m^{-3}$ for thermokarst deposits) is caused by syngenetic permafrost formation in polygonal tundra landscapes over long periods in the Quaternary (Schirrmeister et al., 2013). However, comparing the studied deposits to the overall Yedoma region mean ($19\,kgC\,m^{-3}$ for Yedoma deposits and $33\,kgC\,m^{-3}$ (disregarding wedge-ice content) for thermokarst deposits; Strauss et al., 2013) on the Buor-Khaya Peninsula reveals that both deposit types contain less OC. Nevertheless, these numbers show that such deposits comprise a large pool of dormant carbon, which could be reactivated due to permafrost thawing. Moreover, thermokarst deposits seem to be the quantitatively more important OC pool (Yedoma : thermokarst carbon ratio $\sim 2:3$). The higher carbon inventory in thermokarst deposits is partially related to a concentration effect for reworked Yedoma OC due to thaw subsidence progression, including ground ice loss plus the input of Holocene OC. Together with ecosystem recovery, thermokarst basins can act as a local sink for portions of the carbon released from thawing permafrost deposits (van Huissteden and Dolman, 2012). Nevertheless, at the same time, thermokarst lakes also promote intense organic-matter degradation, including methane production in the anaerobic environments of organically rich lake sediments and unfrozen deposits (Walter et al., 2007b; Shirokova et al., 2013). To answer the question raised in the introduction of whether the thermokarst organic-matter pool is as degradable as the

frozen late Pleistocene Yedoma, we visualized the stratigraphically differentiated main proxies in Fig. 7.

In our study the C / N data show some overlap (Fig. 7b). The average values are relatively close together for all profiles, but the differences are statistically significant (Table S1). Thus, the C / N medians and means suggest a lower degradation state or better organic-matter quality of thermokarst deposits (especially Buo-05 and Buo-03). Moreover, in both Yedoma and thermokarst deposits, the same pattern is visible: a positive linear relationship exists between $TOC_{wt\,\%}$ and C / N ratios (Fig. 5b). In soil science literature, it is agreed that the elemental composition of organic matter is affected by the degree of humification and microbial activity that metabolize the organic matter (Kumada, 1987). Ongoing organic-matter decomposition will release stored C to the atmosphere and N to the soil (Weintraub and Schimel, 2005), resulting in a lower C / N ratio for more degraded deposits (Gundelwein et al., 2007). This was found in (sub-) Arctic peat deposits and soils, where the C / N ratio decreases with depth (Kuhry and Vitt, 1996; McKane et al., 1997; Ping et al., 1998). Because a high TN content can promote the stabilization of organic matter at late stages of decomposition (Berg, 2000), this further supports the interpretation that a low C / N ratio indicates recalcitrant or matured organic matter (Rumpel and Kögel-Knabner, 2011). Schädel et al. (2014) found, in incubation studies, that the C / N ratio is a good estimator for organic-matter decomposability and vulnerability. Although the C / N ratios are lower than in Arctic peat deposits (Hugelius et al., 2012; Routh et al., 2014), the ratios are still in the range of or higher than those found in many other deep mineral soils of the temperate zone (Jenkinson et al., 2008; Rumpel and Kögel-Knabner, 2011). Thus, both Yedoma and thermokarst deposits show relatively good organic-matter quality for microbial decay after becoming available by thaw. The C / N ratios, especially for the paleocryosols, suggest that good quality organic matter was preserved (by temperature near or below 0 °C during thermokarst processes) for future decomposition. This is shown by the δ^{13}C ratio as well. Neglecting the influence of different sources of organic matter on the δ^{13}C ratio, which is justified by constant ACL values of > 28 (higher land plants, Fig. S4) for Yedoma and thermokarst deposits, the δ^{13}C ratio is an appropriate proxy for estimating the intrinsic state of degradation. Therefore, the δ^{13}C values indicate a significantly lower organic-matter degradation for the thermokarst samples, implying a better quality than that found in Yedoma samples. The high CPI values of the thermokarst and the Yedoma organic matter (around 9 and higher) indicate fresh and less degraded terrigenous organic matter (Brassell et al., 1978) for both deposits (Fig. 7d). The CPI values of the Yedoma deposit organic matter, which are (significantly) higher than in the thermokarst deposits, indicate a better quality for further decomposition (Fig. 7d).

Routh et al. (2014) states that other, more labile compounds like *n*-alcohols and *n*-fatty acids are degraded to *n*-

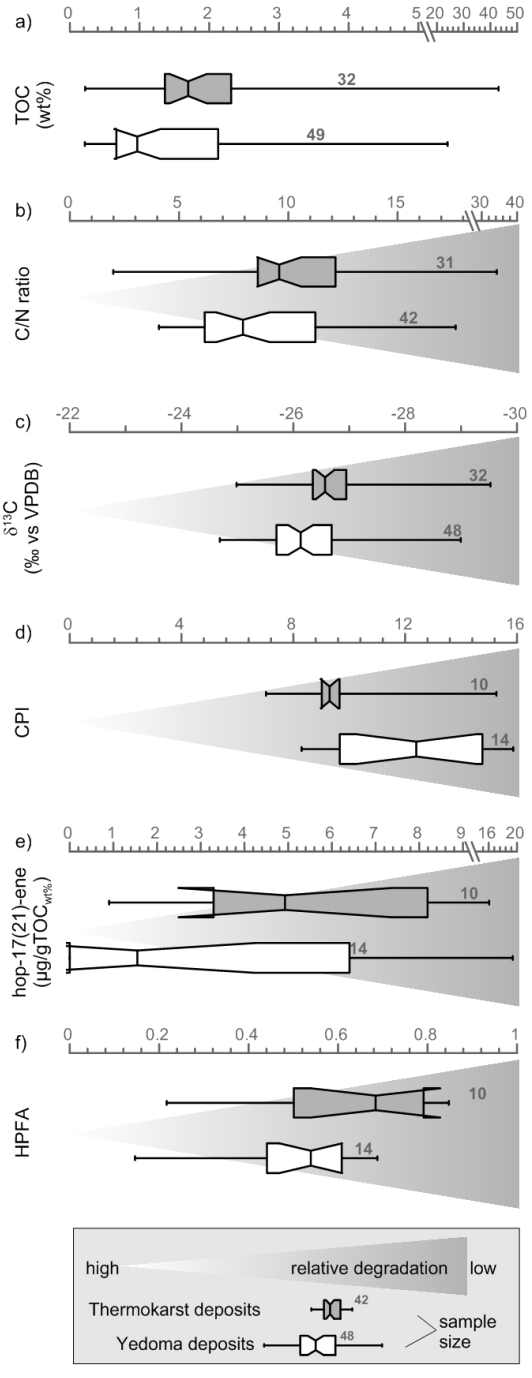

Figure 7. Conceptual scheme of the organic-matter degradation state, estimated using the different applied proxies with boxplots. The merged profiles of Yedoma deposit boxplots (white boxes) are shown below the thermokarst deposits (grey boxes). The whiskers illustrate the data range, and the box ends indicate the 25th and the 75th quartile (interquartile range). The vertical lines inside each box show the median (= 50th quartile), including the 95 % confidence intervals, represented by notches. Grey numbers show the sample size. All diagrams are drawn in such a way as to show more degraded samples on the left and less degraded samples on the right side. Thus, the axis of δ^{13}C shows descending values.

alkanes. Thus, an increase in *n*-alkanes (Figs. 3 and 4, absolute lipid concentration column) is an indicator for cumulative decay. We do not see a decreasing trend, which points to a constantly low decomposition state. In addition, no increasing *n*-fatty-acid CPI with depth (as was shown in an Arctic peat by Andersson and Meyers, 2012) was obvious. Andersson and Meyers (2012) interpreted this to reflect fatty-acid production during humification, but we do not see this humification effect in our data, neither in Yedoma nor in the thermokarst deposits. Moreover, as indicated by the dominance of long-chain *n*-alkane and *n*-fatty-acid compounds vs. compounds of shorter chain length (Höfle et al., 2013), we confirm the interpretation that there is good organic-matter preservation in both Yedoma and thermokarst deposits. At first view, the hop-17(21)-ene (Fig. 7e) concentration does not show a significant preservation difference between both kinds of deposits because the Buo-04 Yedoma profile contains hopene concentrations in the same range as those found in thermokarst deposits. However, if we focus on the median values, the Yedoma deposits again appear to be slightly more degraded than the thermokarst deposits. With the exception of Buo-01, the HPFA index (Fig. 7f) also suggests lower degradation and better organic-matter quality in the thermokarst deposit profiles (Buo-05 and Buo-03). Our HPFA index, introduced based on the HPA index of Poynter (1989), which was tested in the Arctic environment by Routh et al. (2014), is an appropriate indicator of the relative amount of the labile fatty acids that remain in a sample. The uppermost samples just below the surface at Buo-04, Buo-05, and Buo-01 and with lower HPFA values are clearly an exception and suggest the entrainment of higher proportions of material influenced by Holocene degradation. This is likely caused by the fairly recent influence of an active layer or transient layer and warmer permafrost temperatures. The oleanene ratio shows a separation of Yedoma and thermokarst deposits, but this ratio is dominated by numerous 0.0 measurements in the Yedoma deposits. These results might be caused not only by the transformation of β-amyrin to olean-12-ene (by losing the hydroxyl group) or to olean-13(18)-ene (by losing the double bond) but also by processes so far unknown in the Yedoma deposits. Thus, because of sparse data and to avoid overinterpretation, this proxy is interpreted only as a weak indication of better Yedoma organic-matter quality for further decomposition.

Summing up Fig. 7, thermokarst organic matter is partly less degraded compared to the organic matter sequestered in Yedoma deposits (see Table S1, significance for C / N, δ^{13}C, and the HPFA index). The CPI points in the other direction (Fig. 7 and Table S1). For hop-17(21)-ene, we do not see significant differences. Nevertheless, the interquartile ranges show an overlap for most proxies. We interpret this in the following way: compared to unaltered Yedoma deposits, degradation during thermokarst processes, but also heightened amounts of OC input during climatically more favorable Holocene times, balance each other out with regard to the organic-matter quality for future degradation. Nevertheless, as there is more carbon stored in the thermokarst basins (Strauss et al., 2013), thermokarst deposits imply a higher intrinsic potential to contribute greenhouse gases in a warmer future. This is supported by the acetate data indicating a higher mean content for the thermokarst deposits. Acetate is an excellent substrate for microbial turnover, e.g., acetoclastic methanogenesis (Kotsyurbenko et al., 2004). The PCA confirms this picture that shows little difference between the organic-matter preservation of the Yedoma and the thermokarst samples. Especially Fig. 6a, supported by Fig. 2, reveals that Yedoma and thermokarst deposits are composed of similar sediments. The Buo-05 thermokarst profile is very similar to both Yedoma profiles. The PCA of the degradation proxies (Fig. 6b) also shows no clusters but exhibits slightly better separation between both kinds of deposits. Figure 6b reveals that the C / N ratio, the δ^{13}C ratio, and the CPI are correlated. This is also separately illustrated in Fig. 5a and c. Thus, these proxies seem to confirm each other. The PCA of the *n*-alkane chain length points to a potential dominance of longer-chain alkanes in Yedoma and shorter-chain alkanes in thermokarst, indicating better quality for further decomposition of Yedoma samples (Höfle et al., 2013). Exceptions are the Buo-05-A-01 and Buo-03-A-03 thermokarst samples, which point in the same direction as the n-C_{35} concentration.

The abovementioned overlap of the interquartile range (Fig. 7) and especially the PCA of the biomarkers (Fig. 6b and c) show that the organic-matter degradation and decomposition vulnerability is heterogeneous and depends on different decomposition trajectories and differing former decomposition and incorporation histories. This is likely shown in both Yedoma and thermokarst deposits, covering the whole range of degradation proxy values (Fig. 7b, c, e). To elucidate this was one of the benefits of the applied multi-proxy approach. With the addition of biomarker data, it is possible to show that the permafrost organic-matter degradation is not a linear function of age or sediment facies but likely a combination of (interrupted) degradation cycles and a cascade of degradation steps. In particular, the reasonably good organic-matter preservation of thermokarst deposits reveals that the sediment degradation processes do not necessarily degrade the organic matter. Potentially, the loss of labile OC during thermokarst processes was compensated for by high rates of Holocene OC accumulation in, e.g., lake sediments. Nutrient release from thawing permafrost could have stimulated lake productivity, whereas decomposition was slow because of low lake temperatures, resulting in cold anoxic lake environments (Boike et al., 2013; Walter Anthony et al., 2014). When the lake drained, permafrost formation rapidly recovered the sediments (Jones et al., 2011), including any possibly newly accumulated OC.

4.3 Fate of organic matter

The permafrost OC resilience or vulnerability is a topic of recent research (Schuur and Abbott, 2011; Knoblauch et al., 2013; Hodgkins et al., 2014; Li et al., 2014; Mu et al., 2014). Any warming permafrost is potentially vulnerable to thawing. The remaining important question is this: what is the fate of the organic matter exposed to degradation after permafrost has thawed? The lipid biomarker data discussed (CPI etc.) indicate that the organic matter in the sediments was, after initial degradation processes, relatively quickly protected against microbial alteration by freezing. This is confirmed by an absent degradation–depth trend which reveals good organic-matter quality independent of age. Thus, the very old frozen organic matter is also vulnerable to degradation after thawing. This interpretation fits results from studies of permafrost-affected Arctic peats (Hugelius et al., 2012; Routh et al., 2014). Walter Anthony et al. (2014) found a net accumulation in thermokarst basins since the last deglaciation but predict that these will change to a large carbon source when permafrost thaws and the OC will be available for oxidation. Due to ongoing climate warming in the Arctic, Grosse et al. (2011b) supposed an increasing occurrence in and magnitude of disturbance processes, especially fire and thermokarst, which will accelerate permafrost degradation. Because our sedimentological and biomarker proxies show a low degradation state, especially for the paleocryosol sequences, we expect a significant vulnerability to microbial degradation after thawing. As evidence that the OC is vulnerable when thawed, Gaglioti et al. (2014) found that ~ 10 times more ancient OC found in permafrost was made available for degradation during warm times of the Holocene (Holocene Thermal Maximum (11.7–9.0 ka) and Bølling–Allerød periods) than is available today. Through increased disturbances, such as deep surface subsidence caused by thawing and the draining of excess water from melting ice in a warmer climate, the Yedoma and, to a lesser degree because of lower excess ice content, the thermokarst organic matter could become bioavailable deep in the sediment. The wedge-ice volume is estimated to be up to ~ 60 vol % for Yedoma and up to ~ 10 vol % for thermokarst deposits (Ulrich et al., 2014). When added to segregated ice, ~ 80 and ~ 65 vol % mean sedimentary ice volume exists in Yedoma and thermokarst, respectively (Strauss et al., 2013). When it becomes available and is exported as dissolved OC to, e.g., river systems, Vonk et al. (2013) and Mann et al. (2014) found that dissolved OC (< 0.45 µm) in ancient Yedoma is exceptionally biolabile. However, if it is not dissolved, the suspended (> 0.45 µm) eroded ancient organic matter could be protected from extensive degradation by organo-mineral bonds, which stabilize the organic matter (Höfle et al., 2013) and, in an aquatic environment, promote rapid settling because they weigh down the organic matter (Vonk et al., 2010).

From the modeling perspective, global-scale models have, so far, been limited because they implement one-dimensional vertical thaw only (Koven et al., 2011; Schneider von Deimling et al., 2012; Schaphoff et al., 2013). Thus, the potentially labile Yedoma and thermokarst deep OC pool described in this study is not realistically implemented in these models because the models disregard rapid phenomena, such as thermokarst processes. Thermokarst processes, despite being local in nature, are widespread on the regional scale (Grosse et al., 2011a) and may constitute the crucial process making the deep OC studied here microbiologically available.

5 Conclusions

Being freeze-locked, a great amount of organic matter in the studied sediments is highly decomposable. Generally, in all applied proxies there is no degradation–depth trend obvious, revealing that permafrost acts like a freezer, preserving the organic matter after freezing. Based on interpreting the mean values of the C / N ratio, isotope ratio (δ^{13}C), and the HPFA index, the thermokarst organic matter is less degraded and of better quality for degradation after thawing compared to the organic matter sequestered in Yedoma deposits. The CPI data suggest less degradation of the organic matter from both deposits, with a higher value for Yedoma organic matter. For the hop-17(21)-ene concentration, no significant difference was found. We do not see any conflict between these two determinations because the interquartile ranges overlap for most proxies. We interpret this as indicating a comparable magnitude of organic-matter quality in both kinds of deposits, but with a likely better thermokarst organic-matter quality for further degradation. For a modeling approach, this conclusion could be extrapolated to the Laptev Sea region as the studied deposits are akin to other Yedoma and thermokarst deposits of the northeast Siberian Arctic (Schirrmeister et al. 2011a).

The fate of mobilized Yedoma deposit OC depends largely on the environmental conditions that exist during the thermokarst processes and in the resulting thermokarst basin. In conclusion, when the conditions during the thermokarst processes are good for organic-matter preservation, for example cold (slightly above 0 °C) or anoxic (lake) conditions, and when reworked fossil organic matter can rapidly refreeze to permafrost, good-quality organic matter for further decomposition can be maintained and inputs likely compensate for losses due to thermokarst degradation.

The Supplement related to this article is available online at doi:10.5194/bg-12-2227-2015-supplement.

Author contributions. J. Strauss, L. Schirrmeister, and S. Wetterich sampled and coordinated all sediment sampling at the Buor-Khaya field campaign in 2010. K. Mangelsdorf supported the biomarker

analysis and interpretation. J. Strauss carried out the laboratory analyses, except for one profile, which was analyzed by L. Eichhorn. U. Herzschuh designed the statistical analyses. J. Strauss planned and wrote the publication with input from all co-authors.

Acknowledgements. We acknowledge support of this research by the German Ministry of Education and Research (the "System Laptev Sea" and "CarboPerm" (03G0836A) projects). We also thank the Russian and German partners who were involved in the "Eastern Laptev Sea – Buor Khaya Peninsula 2010" expedition. J. Strauss was supported by a grant from the Studienstiftung des deutschen Volkes (German National Academic Foundation), the European Research Council Starting Grant (PETA-CARB, #338335), and the Initiative and Networking Fund of the Helmholtz Association (#ERC-0013).

Edited by: D. Obrist

References

Andersson, R. A. and Meyers, P. A.: Effect of climate change on delivery and degradation of lipid biomarkers in a Holocene peat sequence in the eastern European Russian Arctic, Org. Geochem., 53, 63–72, doi:10.1016/j.orggeochem.2012.05.002, 2012.

Andersson, R. A., Kuhry, P., Meyers, P., Zebühr, Y., Crill, P., and Mörth, M.: Impacts of paleohydrological changes on n-alkane biomarker compositions of a holocene peat sequence in the eastern European Russian Arctic, Org. Geochem., 42, 1065–1075, doi:10.1016/j.orggeochem.2011.06.020, 2011.

Berg, B.: Litter decomposition and organic matter turnover in northern forest soils, Forest Ecol. Manag., 133, 13–22, doi:10.1016/S0378-1127(99)00294-7, 2000.

Blott, S. J. and Pye, K.: Gradistat: A grain size distribution and statistics package for the analysis of unconsolidated sediments, Earth Surf. Proc. Land., 26, 1237–1248, doi:10.1002/esp.261, 2001.

Boike, J., Kattenstroth, B., Abramova, K., Bornemann, N., Chetverova, A., Fedorova, I., Fröb, K., Grigoriev, M., Grüber, M., Kutzbach, L., Langer, M., Minke, M., Muster, S., Piel, K., Pfeiffer, E.-M., Stoof, G., Westermann, S., Wischnewski, K., Wille, C., and Hubberten, H.-W.: Baseline characteristics of climate, permafrost and land cover from a new permafrost observatory in the Lena River Delta, Siberia (1998–2011), Biogeosciences, 10, 2105–2128, doi:10.5194/bg-10-2105-2013, 2013.

Brassell, S., Eglinton, G., Maxwell, J., and Philp, R.: Natural background of alkanes in the aquatic environment, in: Aquatic pollutants: Transformation and biological effects, edited by: Hutzinger, O., Lelyveld, I. H., and Zoetman, B. C. J., Pergamon Press, Oxford, 519 pp., 1978.

Bray, E. E. and Evans, E. D.: Distribution of n-paraffins as a clue to recognition of source beds, Geochim. Cosmochim. Ac., 22, 2–15, doi:10.1016/0016-7037(61)90069-2, 1961.

Ciais, P., Tagliabue, A., Cuntz, M., Bopp, L., Scholze, M., Hoffmann, G., Lourantou, A., Harrison, S. P., Prentice, I. C., Kelley, D. I., Koven, C., and Piao, S. L.: Large inert carbon pool in the terrestrial biosphere during the last glacial maximum, Nat. Geosci., 5, 74–79, doi:10.1038/ngeo1324, 2012.

Dlugokencky, E. and Tans, P.: Trends in atmospheric carbon dioxide: available at: http://www.esrl.noaa.gov/gmd/ccgg/trends/global.html, last access 23 March 2014.

Drachev, S. S., Savostin, L. A., Groshev, V. G., and Bruni, I. E.: Structure and geology of the continental shelf of the Laptev Sea, eastern Russian Arctic, Tectonophysics, 298, 357–393, doi:10.1016/S0040-1951(98)00159-0, 1998.

Drozdov, D. S., Rivkin, F. M., Rachold, V., Ananjeva-Malkova, G. V., Ivanova, N. V., Chehina, I. V., Koreisha, M. M., Korostelev, Y. V., and Melnikov, E. S.: Electronic atlas of the Russian Arctic coastal zone, Geo-Mar. Lett., 25, 81–88, doi:10.1007/s00367-004-0189-7, 2005.

Folk, R. L. and Ward, W. C.: Brazos river bar: A study in the significance of grain size parameters, J. Sediment. Petrol., 27, 3–26, 1957.

Gaglioti, B. V., Mann, D. H., Jones, B. M., Pohlman, J. W., Kunz, M. L., and Wooller, M. J.: Radiocarbon age-offsets in an Arctic lake reveal the long-term response of permafrost carbon to climate change, J. Geophys. Res.-Biogeo., 119, 1630–1651, doi:10.1002/2014jg002688, 2014.

Glombitza, C., Mangelsdorf, K., and Horsfield, B.: Maturation related changes in the distribution of ester bound fatty acids and alcohols in a coal series from the New Zealand coal band covering diagenetic to catagenetic coalification levels, Org. Geochem., 40, 1063–1073, doi:10.1016/j.orggeochem.2009.07.008, 2009.

Goslar, T., Czernik, J., and Goslar, E.: Low-energy ^{14}C ams in Poznań radiocarbon laboratory, Poland, Nuclear Instruments and Methods in: Physics Research Section B: Beam Interactions with Materials and Atoms, 223–224, 5–11, doi::10.1016/j.nimb.2004.04.005, 2004.

Grosse, G., Harden, J., Turetsky, M. R., McGuire, A. D., Camill, P., Tarnocai, C., Frolking, S., Schuur, E. A. G., Jorgenson, T., Marchenko, S., Romanovsky, V., Wickland, K. P., French, N., Waldrop, M. P., Bourgeau-Chavez, L., and Striegl, R. G.: Vulnerability of high-latitude soil organic carbon in North America to disturbance, J. Geophys. Res., 116, G00K06, doi:10.1029/2010JG001507, 2011a.

Grosse, G., Romanovsky, V., Jorgenson, T., Anthony, K. W., Brown, J., and Overduin, P. P.: Vulnerability and feedbacks of permafrost to climate change, Eos, Transactions American Geophysical Union, 92, 73–74, doi:10.1029/2011eo090001, 2011b.

Grosse, G., Robinson, J. E., Bryant, R., Taylor, M. D., Harper, W., DeMasi, A., Kyker-Snowman, E., Veremeeva, A., Schirrmeister, L., and Harden, J.: Distribution of late Pleistocene ice-rich syngenetic permafrost of the yedoma suite in east and central Siberia, Russia, U.S. Geological Survey Open File Report, 1078, U.S. Geological Survey, Reston, USA, 37 pp., 2013.

Gubin, S. V. and Veremeeva, A. A.: Parent materials enriched in organic matter in the northeast of Russia, Eurasian Soil Sci., 43, 1238–1243, doi:10.1134/s1064229310110062, 2010.

Gundelwein, A., Muller-Lupp, T., Sommerkorn, M., Haupt, E. T. K., Pfeiffer, E., and Wiechmann, H.: Carbon in tundra soils in the lake labaz region of Arctic Siberia, Eur. J. Soil Sci., 58, 1164–1174, 2007.

Günther, F., Overduin, P. P., Sandakov, A., Grosse, G., and Grigoriev, M. N.: Thermo-erosion along the yedoma coast of the Buor Khaya peninsula, Laptev Sea, east Siberia, Proceedings of the Tenth International Conference on Permafrost, Volume 1: In-

ternational Contributions, Salekhard, Russia, 25–29 June 2012, 137–142, 2012

Günther, F., Overduin, P. P., Sandakov, A. V., Grosse, G., and Grigoriev, M. N.: Short- and long-term thermo-erosion of ice-rich permafrost coasts in the Laptev Sea region, Biogeosciences, 10, 4297–4318, doi:10.5194/bg-10-4297-2013, 2013.

Heyer, J., Hübner, H., and Maaß, I.: Isotopenfraktionierung des Kohlenstoffs bei der mikrobiellen Methanbildung, Isot. Environ. Health S., 12, 202–205, doi:10.1080/10256017608543912, 1976.

Hodgkins, S. B., Tfaily, M. M., McCalley, C. K., Logan, T. A., Crill, P. M., Saleska, S. R., Rich, V. I., and Chanton, J. P.: Changes in peat chemistry associated with permafrost thaw increase greenhouse gas production, P. Natl. Acad. Sci., 111, 5819–5824, doi:10.1073/pnas.1314641111, 2014.

Höfle, S., Rethemeyer, J., Mueller, C. W., and John, S.: Organic matter composition and stabilization in a polygonal tundra soil of the Lena Delta, Biogeosciences, 10, 3145–3158, doi:10.5194/bg-10-3145-2013, 2013.

Hugelius, G., Routh, J., Kuhry, P., and Crill, P.: Mapping the degree of decomposition and thaw remobilization potential of soil organic matter in discontinuous permafrost terrain, J. Geophys. Res.-Biogeo., 117, G02030, doi:10.1029/2011jg001873, 2012.

Hugelius, G., Strauss, J., Zubrzycki, S., Harden, J. W., Schuur, E. A. G., Ping, C.-L., Schirrmeister, L., Grosse, G., Michaelson, G. J., Koven, C. D., O'Donnell, J. A., Elberling, B., Mishra, U., Camill, P., Yu, Z., Palmtag, J., and Kuhry, P.: Estimated stocks of circumpolar permafrost carbon with quantified uncertainty ranges and identified data gaps, Biogeosciences, 11, 6573–6593, doi:10.5194/bg-11-6573-2014, 2014.

Jenkinson, D. S., Poulton, P. R., and Bryant, C.: The turnover of organic carbon in subsoils, Part 1., Natural and bomb radiocarbon in soil profiles from the Rothamsted long-term field experiments, Eur. J. Soil Sci., 59, 391–399, doi:10.1111/j.1365-2389.2008.01025.x, 2008.

Jones, B. M., Grosse, G., Arp, C. D., Jones, M. C., Walter Anthony, K. M., and Romanovsky, V. E.: Modern thermokarst lake dynamics in the continuous permafrost zone, northern Seward Peninsula, Alaska, J. Geophys. Res., 116, G00M03, doi:10.1029/2011JG001666, 2011.

Knoblauch, C., Beer, C., Sosnin, A., Wagner, D., and Pfeiffer, E.-M.: Predicting long-term carbon mineralization and trace gas production from thawing permafrost of northeast Siberia, Glob. Change Biol., 19, 1160–1172, doi:10.1111/gcb.12116, 2013.

Kotsyurbenko, O. R., Chin, K.-J., Glagolev, M. V., Stubner, S., Simankova, M. V., Nozhevnikova, A. N., and Conrad, R.: Acetoclastic and hydrogenotrophic methane production and methanogenic populations in an acidic West-Siberian peat bog, Environ. Microbiol., 6, 1159–1173, doi:10.1111/j.1462-2920.2004.00634.x, 2004.

Koven, C. D., Ringeval, B., Friedlingstein, P., Ciais, P., Cadule, P., Khvorostyanov, D., Krinner, G., and Tarnocai, C.: Permafrost carbon-climate feedbacks accelerate global warming, P. Natl. Acad. Sci., 108, 14769–14774, doi:10.1073/pnas.1103910108, 2011.

Kuesel, K. and Drake, H. L.: Effects of environmental parameters on the formation and turnover of acetate by forest soils, Appl. Environ. Microb., 61, 3667–3675, 1995.

Kuhry, P. and Vitt, D. H.: Fossil carbon/nitrogen ratios as a measure of peat decomposition, Ecology, 77, 271–275, doi:10.2307/2265676, 1996.

Kuhry, P., Ping, C.-L., Schuur, E. A. G., Tarnocai, C., and Zimov, S.: Report from the international permafrost association: Carbon pools in permafrost regions, Permafrost Periglacial Process, 20, 229–234, doi:10.1002/ppp.648, 2009.

Kumada, K.: Chemistry of soil organic matter, Developments in soil science, Elsevier/Japan Scientific Societies Press, Amsterdam, 241 pp., 1987.

Lee, H., Schuur, E. A. G., Inglett, K. S., Lavoie, M., and Chanton, J. P.: The rate of permafrost carbon release under aerobic and anaerobic conditions and its potential effects on climate, Glob. Change Biol., 18, 515–527, doi:10.1111/j.1365-2486.2011.02519.x, 2012.

Li, J., Luo, Y., Natali, S., Schuur, E. A. G., Xia, J., Kowalczyk, E., and Wang, Y.: Modeling permafrost thaw and ecosystem carbon cycle under annual and seasonal warming at an Arctic tundra site in Alaska, J. Geophys. Res.-Biogeo., 119, 1129–1146, doi:10.1002/2013jg002569, 2014.

Luo, Q., Yu, S., Liu, Y., Zhang, Y., Han, H., Qi, L., and Zhong, N.: Existence and implications of hop-17(21)-enes in the lower cretaceous of the Saihantala Sag, Erlian Basin, China, Pet. Sci., 9, 154–160, doi:10.1007/s12182-012-0195-8, 2012.

Mangelsdorf, K., Finsel, E., Liebner, S., and Wagner, D.: Temperature adaptation of microbial communities in different horizons of Siberian permafrost-affected soils from the Lena Delta, Chemie der Erde – Geochemistry, 69, 169–182, doi:10.1016/j.chemer.2009.02.001, 2009.

Mann, P. J., Sobczak, W. V., LaRue, M. M., Bulygina, E., Davydova, A., Vonk, J. E., Schade, J., Davydov, S., Zimov, N., Holmes, R. M., and Spencer, R. G. M.: Evidence for key enzymatic controls on metabolism of Arctic river organic matter, Glob. Change Biol., 20, 1089–1100, doi:10.1111/gcb.12416, 2014.

Marzi, R., Torkelson, B. E., and Olson, R. K.: A revised carbon preference index, Org. Geochem., 20, 1303–1306, doi:10.1016/0146-6380(93)90016-5, 1993.

McKane, R. B., Rastetter, E. B., Shaver, G. R., Nadelhoffer, K. J., Giblin, A. E., Laundre, J. A., and Chapin, F. S.: Climatic effects on tundra carbon storage inferred from experimental data and a model, Ecology, 78, 1170–1187, doi:10.1890/0012-9658(1997)078[1170:ceotcs]2.0.co;2, 1997.

Mu, C., Zhang, T., Schuster, P. F., Schaefer, K., Wickland, K. P., Repert, D. A., Liu, L., Schaefer, T., and Cheng, G.: Carbon and geochemical properties of cryosols on the north slope of Alaska, Cold Reg. Sci. Technol., 100, 59–67, doi:10.1016/j.coldregions.2014.01.001, 2014.

Oksanen, J.: Multivariate analysis of ecological communities in r: Vegan tutorial, University of Oulu, Oulu, 43 pp., 2013.

Ping, C. L., Bockheim, J. G., Kimble, J. M., Michaelson, G. J., and Walker, D. A.: Characteristics of cryogenic soils along a latitudinal transect in Arctic Alaska, J. Geophys. Res.-Atmos., 103, 28917–28928, doi:10.1029/98jd02024, 1998.

Poynter, J.: Molecular stratigraphy: The recognition of palaeoclimatic signals in organic geochemical data, PhD, School of Chemistry, University of Bristol, Bristol, 324 pp., 1989.

Poynter, J. and Eglinton, G.: 14. Molecular composition of three sediments from hole 717c: The Bengal fan, Proceedings of the Ocean Drilling Program: Scientific results, 116, 155–161, 1990.

Radke, M., Willsch, H., and Welte, D. H.: Preparative hydrocarbon group type determination by automated medium pressure liquid chromatography, Anal. Chem., 52, 406–411, doi:10.1021/ac50053a009, 1980.

Romanovskii, N. N., Hubberten, H. W., Gavrilov, A. V., Tumskoy, V. E., and Kholodov, A. L.: Permafrost of the east Siberian Arctic shelf and coastal lowlands, Quaternary Sci. Rev., 23, 1359–1369, doi:10.1016/j.quascirev.2003.12.014, 2004.

Romanovsky, V. E., Smith, S. L., and Christiansen, H. H.: Permafrost thermal state in the polar northern hemisphere during the international polar year 2007–2009: A synthesis, Permafrost Periglacial Process, 21, 106–116, doi:10.1002/ppp.689, 2010.

Routh, J., Hugelius, G., Kuhry, P., Filley, T., Tillman, P. K., Becher, M., and Crill, P.: Multi-proxy study of soil organic matter dynamics in permafrost peat deposits reveal vulnerability to climate change in the European Russian Arctic, Chem. Geol., 368, 104–117, doi:10.1016/j.chemgeo.2013.12.022, 2014.

Rumpel, C. and Kögel-Knabner, I.: Deep soil organic matter – a key but poorly understood component of terrestrial C cycle, Plant Soil, 338, 143–158, doi:10.1007/s11104-010-0391-5, 2011.

Schädel, C., Schuur, E. A. G., Bracho, R., Elberling, B., Knoblauch, C., Lee, H., Luo, Y. Q., Shaver, G. R., and Turetsky, M. R.: Circumpolar assessment of permafrost C quality and its vulnerability over time using long-term incubation data, Glob. Change Biol., 20, 641–652, doi:10.1111/gcb.12417, 2014.

Schaphoff, S., Heyder, U., Ostberg, S., Gerten, D., Heinke, J., and Lucht, W.: Contribution of permafrost soils to the global carbon budget, Environ. Res. Lett., 8, 014026, doi:10.1088/1748-9326/8/1/014026, 2013.

Schirrmeister, L., Grosse, G., Wetterich, S., Overduin, P. P., Strauss, J., Schuur, E. A. G., and Hubberten, H.-W.: Fossil organic matter characteristics in permafrost deposits of the northeast Siberian Arctic, J. Geophys. Res., 116, G00M02, doi:10.1029/2011jg001647, 2011a.

Schirrmeister, L., Kunitsky, V., Grosse, G., Wetterich, S., Meyer, H., Schwamborn, G., Babiy, O., Derevyagin, A., and Siegert, C.: Sedimentary characteristics and origin of the late pleistocene ice complex on north-east Siberian Arctic coastal lowlands and islands – a review, Quatern. Int., 241, 3–25, doi:10.1016/j.quaint.2010.04.004, 2011b.

Schirrmeister, L., Froese, D. G., Tumskoy, V., Grosse, G., and Wetterich, S.: Yedoma: late Pleistocene ice-rich syngenetic permafrost of Beringia, in: Encyclopedia of quaternary sciences, 2 ed., edited by: Elias, S. A., Quaternary glaciation cold regions landforms, Elsevier, Amsterdam, 542–552, 2013.

Schneider von Deimling, T., Meinshausen, M., Levermann, A., Huber, V., Frieler, K., Lawrence, D. M., and Brovkin, V.: Estimating the near-surface permafrost-carbon feedback on global warming, Biogeosciences, 9, 649–665, doi:10.5194/bg-9-649-2012, 2012.

Schulte, S., Mangelsdorf, K., and Rullkötter, J.: Organic matter preservation on the Pakistan continental margin as revealed by biomarker geochemistry, Org. Geochem., 31, 1005–1022, doi:10.1016/S0146-6380(00)00108-X, 2000.

Schuur, E. A. G. and Abbott, B.: High risk of permafrost thaw, Nature, 480, 32–33, doi:10.1038/480032a, 2011.

Schuur, E. A. G., Vogel, J. G., Crummer, K. G., Lee, H., Sickman, J. O., and Osterkamp, T. E.: The effect of permafrost thaw on old carbon release and net carbon exchange from tundra, Nature, 459, 556–559, doi:10.1038/nature08031, 2009.

Shirokova, L. S., Pokrovsky, O. S., Kirpotin, S. N., Desmukh, C., Pokrovsky, B. G., Audry, S., and Viers, J.: Biogeochemistry of organic carbon, CO_2, CH_4, and trace elements in thermokarst water bodies in discontinuous permafrost zones of Western Siberia, Biogeochemistry, 113, 573–593, doi:10.1007/s10533-012-9790-4, 2013.

Smith, M. R. and Mah, R. A.: Acetate as sole carbon and energy source for growth of methanosarcina strain 227, Appl. Environ. Microb., 39, 993–999, 1980.

Sollins, P., Spycher, G., and Glassman, C. A.: Net nitrogen mineralization from light- and heavy-fraction forest soil organic matter, Soil Biol. Biochem., 16, 31–37, doi:10.1016/0038-0717(84)90122-6, 1984.

Stevenson, F. J.: Humus chemistry: Genesis, composition, reactions, John Wiley & Sons, New York, 512 pp., 1994.

Strauss, J. and Schirrmeister, L.: Permafrost sequences of buor khaya peninsula, in: Reports on polar and marine research – Russian-German cooperation system Laptev Sea: The expedition eastern Laptev Sea-Buor Khaya Peninsula 2010, edited by: Wetterich, S., Overduin, P. P., and Grigoriev, M., Alfred Wegener Institute for Polar and Marine Research, Bremerhaven, Germany, 35–50, 2011.

Strauss, J., Schirrmeister, L., Wetterich, S., Borchers, A., and Davydov, S. P.: Grain-size properties and organic-carbon stock of yedoma ice complex permafrost from the Kolyma lowland, northeastern Siberia, Global Biogeochem. Cy., 26, GB3003, doi:10.1029/2011GB004104, 2012.

Strauss, J., Schirrmeister, L., Grosse, G., Wetterich, S., Ulrich, M., Herzschuh, U., and Hubberten, H.-W.: The deep permafrost carbon pool of the yedoma region in Siberia and Alaska, Geophys. Res. Lett., 40, 6165–6170, doi:10.1002/2013GL058088, 2013.

Stuiver, M., Reimer, P., and Reimer, R.: Calib 6.0, in, ^{14}C CHRONO Centre, Queens University Belfast, Belfast, 2010.

Tieszen, L.: Photosynthesis and respiration in Arctic tundra grasses: Field light intensity and temperature responses, Arctic Alpine Res., 5, 239–251, 1973.

Ulrich, M., Grosse, G., Strauss, J., and Schirrmeister, L.: Quantifying wedge-ice volumes in yedoma and thermokarst basin deposits, Permafrost Periglacial Process, 25, 151–161, doi:10.1002/ppp.1810, 2014.

van Huissteden, J. and Dolman, A. J.: Soil carbon in the Arctic and the permafrost carbon feedback, Current Opinion in Environmental Sustainability, 4, 545–551, doi:10.1016/j.cosust.2012.09.008, 2012.

Vieth, A., Mangelsdorf, K., Sykes, R., and Horsfield, B.: Water extraction of coals – potential for estimating low molecular weight organic acids as carbon feedstock for the deep terrestrial biosphere, Org. Geochem., 39, 985–991, doi:10.1016/j.orggeochem.2008.02.012, 2008.

Vonk, J. E., Sánchez-García, L., Semiletov, I., Dudarev, O., Eglinton, T., Andersson, A., and Gustafsson, Ö.: Molecular and radiocarbon constraints on sources and degradation of terrestrial organic carbon along the Kolyma paleoriver transect, East Siberian Sea, Biogeosciences, 7, 3153–3166, doi:10.5194/bg-7-3153-2010, 2010.

Vonk, J. E., Mann, P. J., Davydov, S., Davydova, A., Spencer, R. G. M., Schade, J., Sobczak, W. V., Zimov, N., Zimov, S., Bulygina, E., Eglinton, T. I., and Holmes, R. M.: High biolability of ancient

permafrost carbon upon thaw, Geophys. Res. Lett., 40, 2689–2693, doi:10.1002/grl.50348, 2013.

Waldrop, M. P., Wickland, K. P., White, R., Berhe, A. A., Harden, J. W., and Romanovsky, V. E.: Molecular investigations into a globally important carbon pool: Permafrost-protected carbon in Alaskan soils, Glob. Change Biol., 16, 2543–2554, doi:10.1111/j.1365-2486.2009.02141.x, 2010.

Walter Anthony, K. M., Zimov, S. A., Grosse, G., Jones, M. C., Anthony, P. M., Chapin, F. S., Finlay, J. C., Mack, M. C., Davydov, S., Frenzel, P., and Frolking, S.: A shift of thermokarst lakes from carbon sources to sinks during the Holocene epoch, Nature, 511, 452–456, doi:10.1038/nature13560, 2014.

Walter, K. M., Edwards, M. E., Grosse, G., Zimov, S. A., and Chapin, F. S.: Thermokarst lakes as a source of atmospheric CH_4 during the last deglaciation, Science, 318, 633–636, doi:10.1126/science.1142924, 2007a.

Walter, K. M., Smith, L. C., and Chapin, S. F.: Methane bubbling from northern lakes: Present and future contributions to the global methane budget, Philos. T. R. Soc. A, 365, 1657–1676, doi:10.1098/rsta.2007.2036, 2007b.

Weintraub, M. N. and Schimel, J. P.: Nitrogen cycling and the spread of shrubs control changes in the carbon balance of Arctic tundra ecosystems, BioScience, 55, 408–415, doi:10.1641/0006-3568(2005)055[0408:ncatso]2.0.co;2, 2005.

Zanina, O. G., Gubin, S. V., Kuzmina, S. A., Maximovich, S. V., and Lopatina, D. A.: Late-Pleistocene (MIS 3-2) palaeoenvironments as recorded by sediments, palaeosols, and ground-squirrel nests at Duvanny Yar, Kolyma Lowland, northeast Siberia, Quaternary Sci. Rev., 30, 2107–2123, doi:10.1016/j.quascirev.2011.01.021, 2011.

Supplement of Biogeosciences, 12, 2227–2245, 2015
http://www.biogeosciences.net/12/2227/2015/
doi:10.5194/bg-12-2227-2015-supplement

Biogeosciences Open Access

Supplement of

Organic-matter quality of deep permafrost carbon – a study from Arctic Siberia

J. Strauss et al.

Correspondence to: J. Strauss (jens.strauss@awi.de)

S1 Supplementary methods

S1.1 Grain-size analyses

To disaggregate the sample and to measure only clastic grains, organic components were removed by adding 35 % hydrogen peroxide three times a week to the samples. The samples were continuously shaken (Innova 2300, New Brunswick) for 6 weeks. The organic-free samples were 'washed' to neutral pH values by repeated decantation after centrifugation (Heraeus Cryofuge 8500i, Thermo Scientific). Samples were dispersed in 1% ammonia solution and 1 g dispersing agent ($Na_4P_2O_7 \times 10H_2O$) and shaken (RS12 Rotoshake, Gerhardt) for at least 5 hours. Finally, each sample was split by a rotary cone sample divider (Laborette 27, Fritsch) and two sub-samples of each main sample were analyzed using a laser particle sizer (LS 200, Beckmann-Coulter). Grain sizes between 0.375 and 1000 µm were determined (Fig. 2, S1). Because no grain fractions >1000 µm occurred, there was no need for fraction reintegration. Grain-size calculations were done after Folk and Ward (1957) using Gradistat v8 (Blott and Pye, 2001).

S1.2 Elemental composition

To determine the total elemental carbon and total nitrogen (TN) content, the samples were freeze-dried (sublimator 3-4-5, Zirbus Technology) and homogenized by grinding (Pulverisette 5 planetary mill, Fritsch) before being measured by a carbon-nitrogen-sulphur analyzer (Vario EL III, Elementar). Two 5 mg sub-samples per sample were taken and encapsulated in two zinc capsules. For ensuring complete oxidation of the sample during measurements ~10 mg of tungsten-(VI)-oxide was added. Background signals were detected by measuring a blank capsule at the beginning and calibration standards after each 20 samples. The quantified measurement accuracy is <± 0.1 wt %. $TOC_{wt\%}$ was measured with a TOC analyzer (Vario Max C, Elementar). Therefore, depending on the previously measured TC content, up to 100 mg were weighed in a crucible and analyzed. The C/N ratio was calculated as the quotient of $TOC_{wt\%}$ and TN values. The volumetric TOC content (TOC_{kg/m^3}) was calculated according to Strauss et al. (2013).

S1.3 Bulk density and volumetric carbon content

Bulk density (BD) measurements were performed in two steps; (1) in the field lab by determining the volume of frozen samples with the Archimedes Principle (quantifying the water displaced in a water-filled glass beaker using a balance (FCB 8K0.1, Kern; accuracy ±0.1 g), and (2) in the freeze-dried laboratory samples; BD was calculated using equation 1. Estimating the BD is required to convert the measured-weight-based $TOC_{wt\%}$ content per sample to a volume-based value. Thus, the TOC_{kg/m^3} was calculated according to equation 2.

S1.4 Carbon isotope studies

Stable TOC carbon isotopes were determined with a Finnigan MAT Delta-S mass spectrometer combined with a FLASH elemental analyzer and a CONFLO III gas mixing system. Before analysis, samples were treated with hydrochloric acid (1.3 molar) and heated at 97°C for three hours to remove the carbonate. After that, the samples were washed to a neutral pH value, dried, and weighed in silver capsules. The sub-sample mass was dependent upon $TOC_{wt\%}$ content of each sample. The $\delta^{13}C$ value was determined by the ratio of ^{13}C to ^{12}C atoms expressed in per mille (‰). In order to quantify the deviations of the $^{13}C/^{12}C$ ratios, the international standard Vienna Pee Dee Belemnite (VPDB) is used.

Ages were determined by radiocarbon dating of selected macroscopic plant remains. The present measurements were performed at the Poznań Radiocarbon Laboratory, Poland, using compact carbon accelerator mass spectrometry (AMS) (Goslar et al., 2004). The presented radiocarbon ages are uncalibrated ages; Table 1 includes calibrated ages as well. Radiocarbon ages are given in year before present (a BP).

S2 Supplementary figures

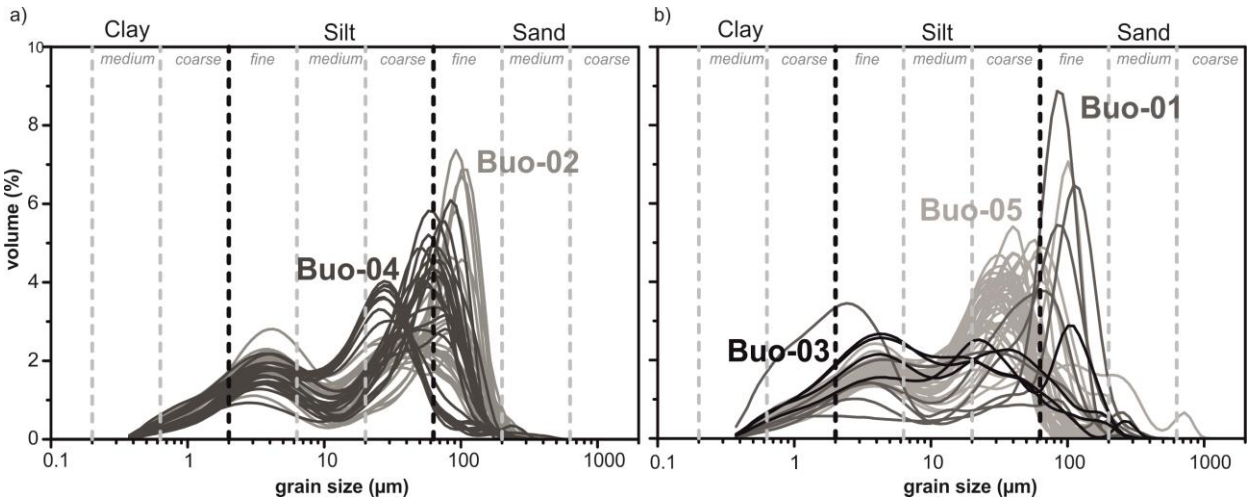

Figure S1. Grain-size distribution of a) Yedoma and b) thermokarst profiles. The different profiles are visualized in different shades of grey.

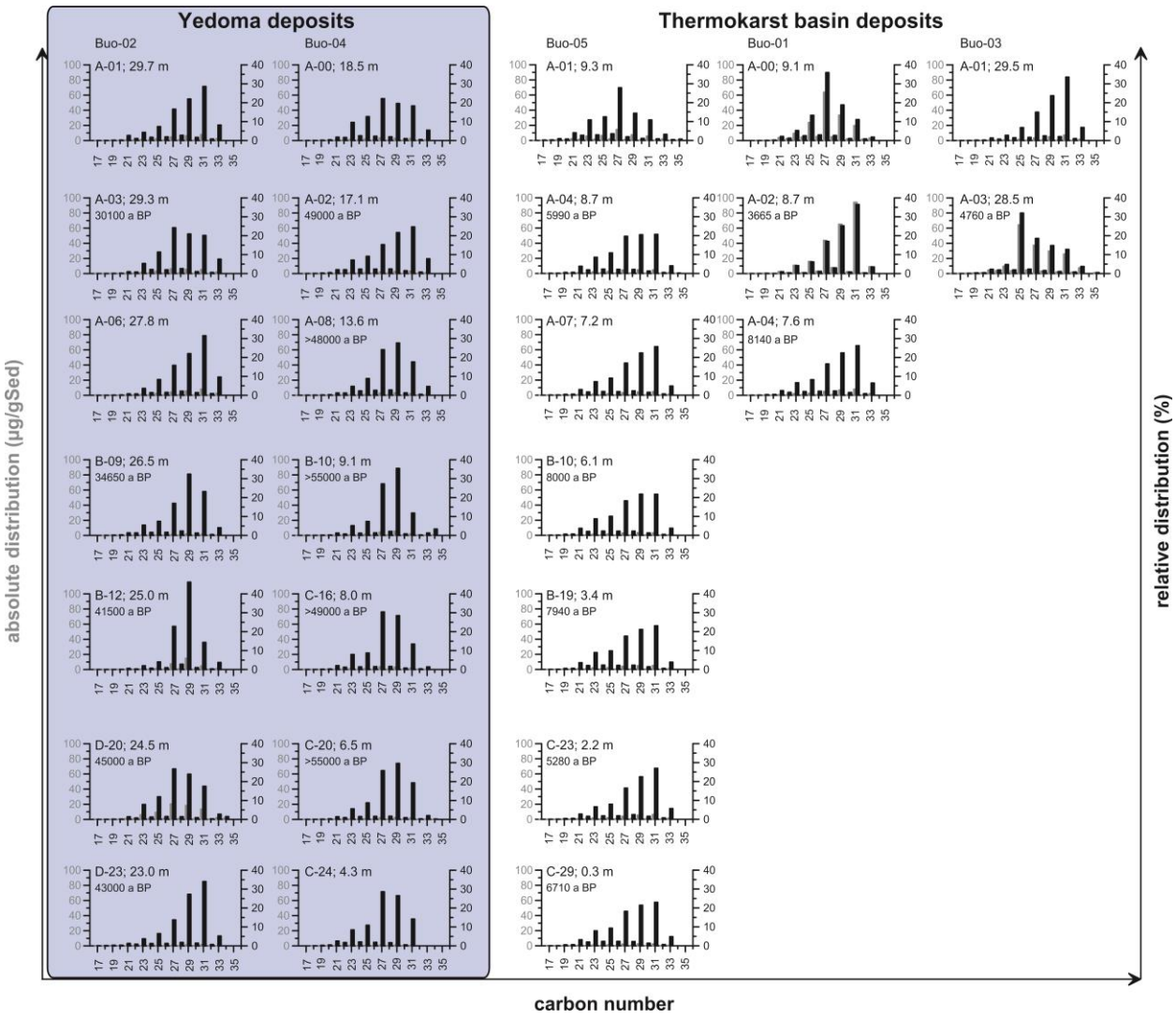

Figure S2. Histogram of the *n*-alkanes. The histograms are sorted stratigraphically from left (old) to right (young). The histograms of the Yedoma deposits are visualized with a blue background.

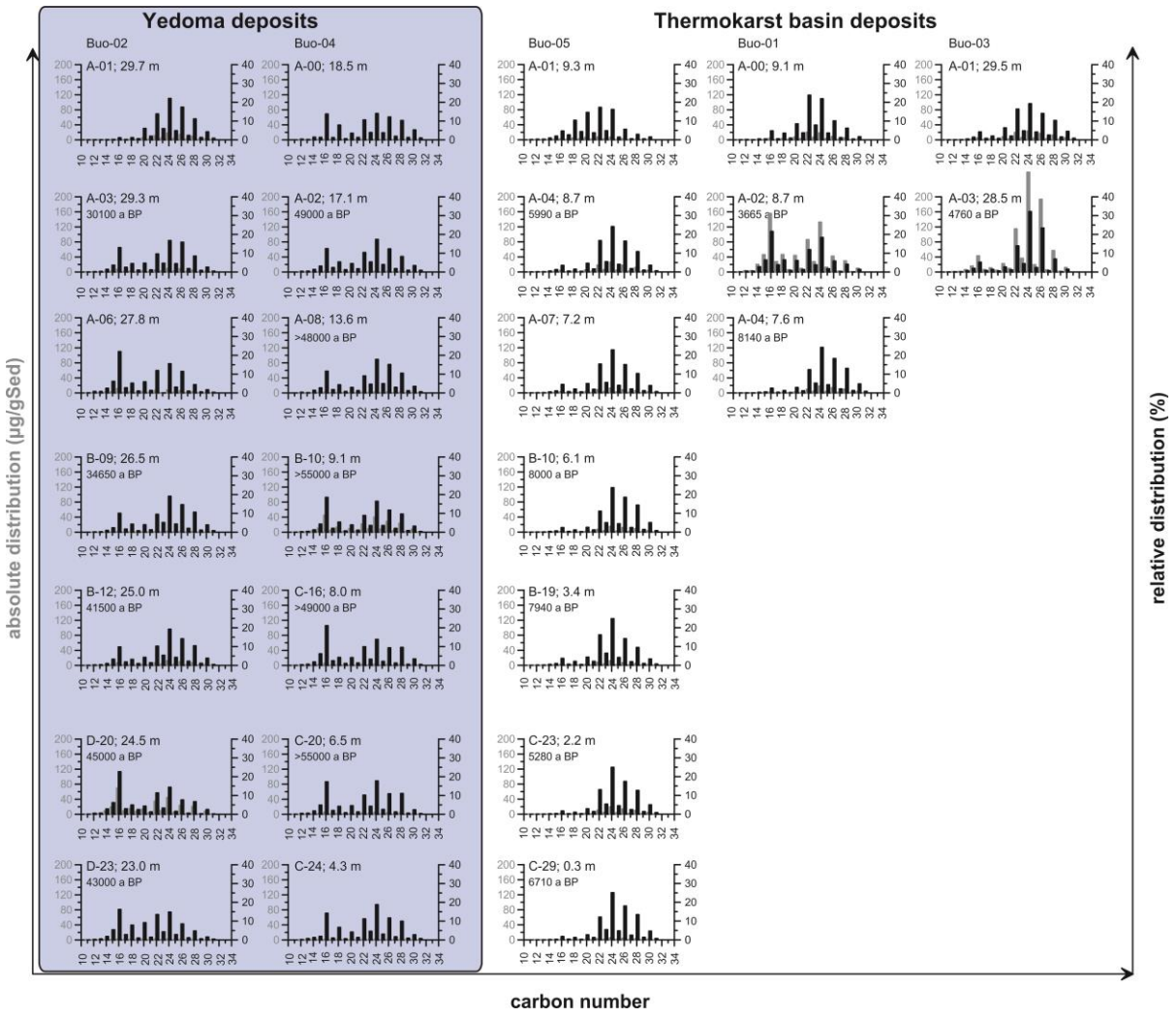

Figure S3. Histogram of the *n*-fatty acids. The histograms are sorted stratigraphically from left (old) to right (young). The histograms of the Yedoma deposits are visualized with a blue background.

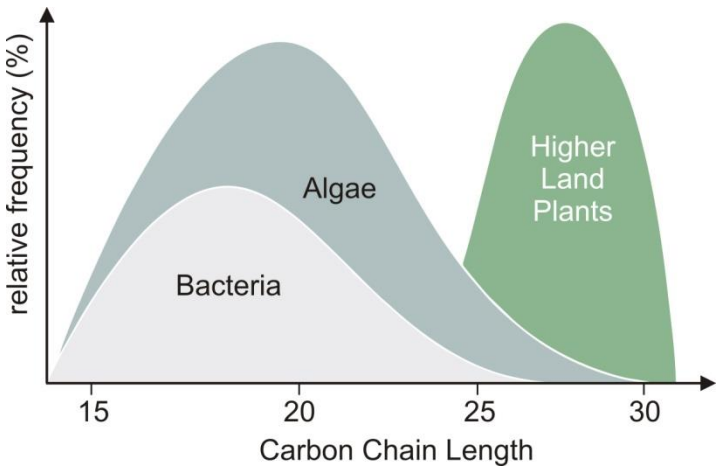

Figure S4. Rough schematic of *n*-alkane chain length in different organisms, modified after Killops and Killops (2009)**.**

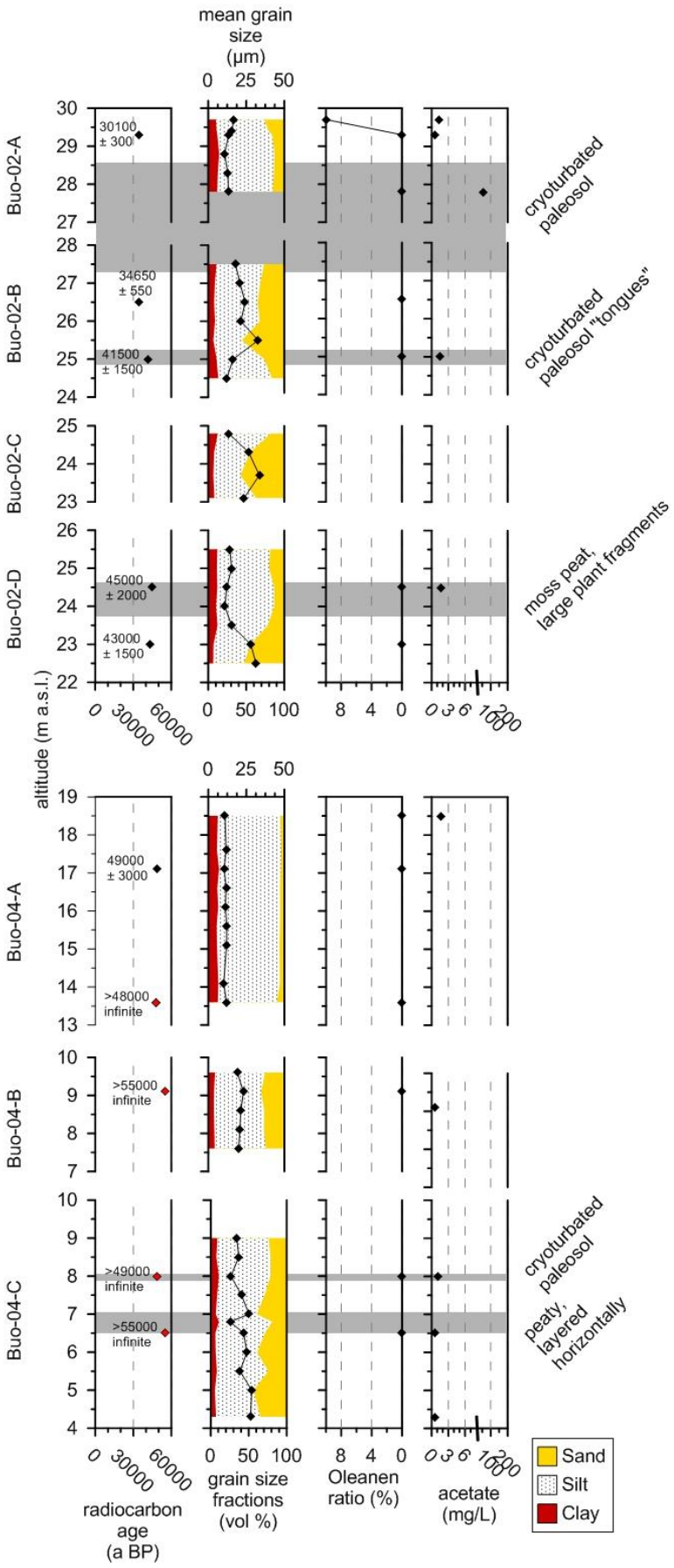

Figure S5. Summary of additional sedimentological and biomarker parameters for the Buo-04 and Buo-02 Yedoma profiles. All diagrams are drawn in such a way as to show more degraded samples on the left and less degraded samples on the right side. Thus, the axis of the Oleanen ratio is descending. In the text, the paleocryosol parts are reported with altitude measurements from the lowest to the highest sample of each paleocryosol. The grey shaded areas are for visualization, not for exact height estimations of the paleocryosols.

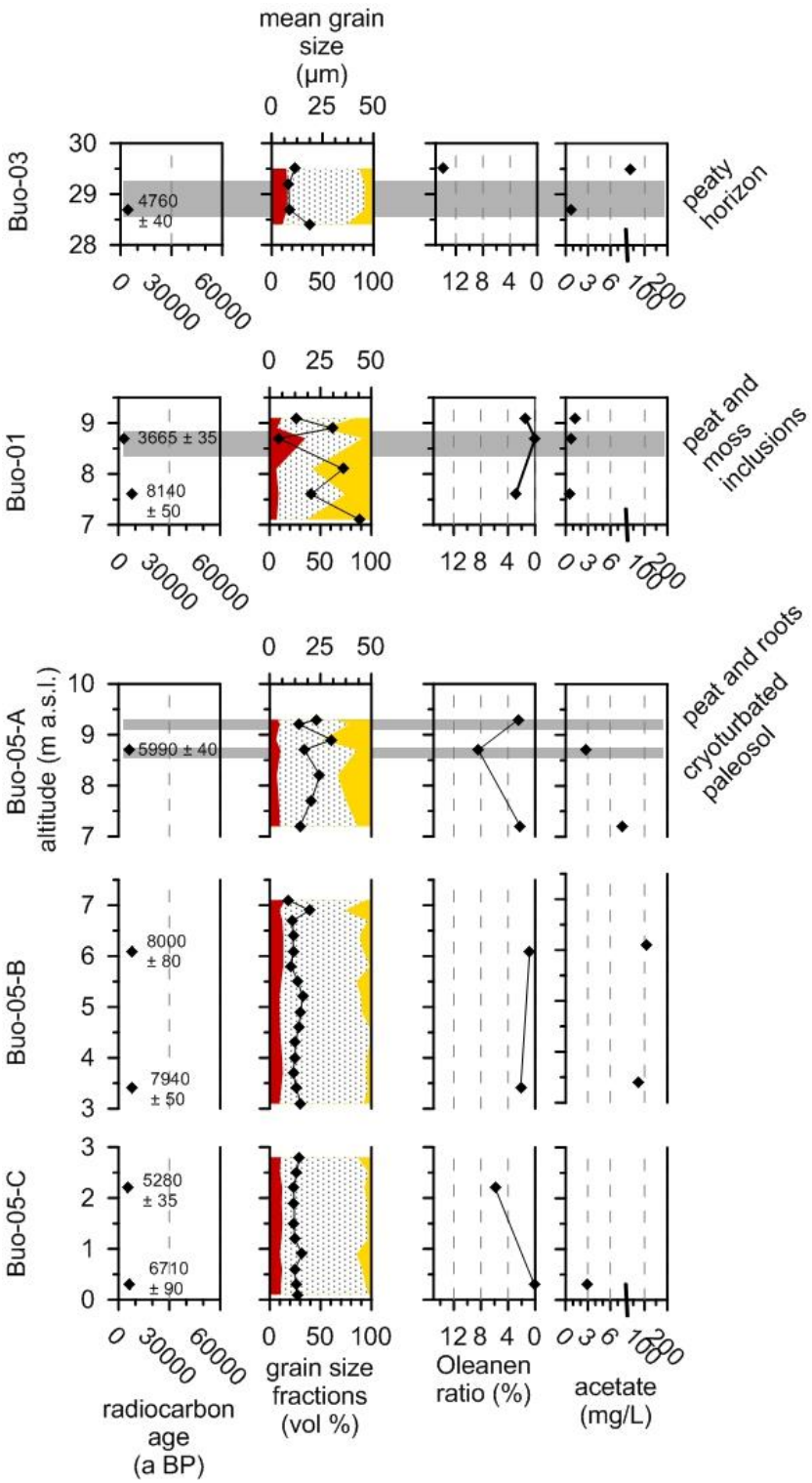

Figure S6. Summary of additional sedimentological and biomarker parameters for the Buo-05, Buo-01, and Buo-03 thermokarst profiles. The grain-size colors are explained in Fig. S5. All diagrams are drawn in such a way as to show more degraded samples on the left and less degraded samples on the right side (descending axis of Oleanen ratio). In the text, the paleocryosol parts are reported with altitude measurements from the lowest to the highest sample of each paleocryosol. The grey shaded areas are for visualization, not for exact height estimations of the paleocryosols.

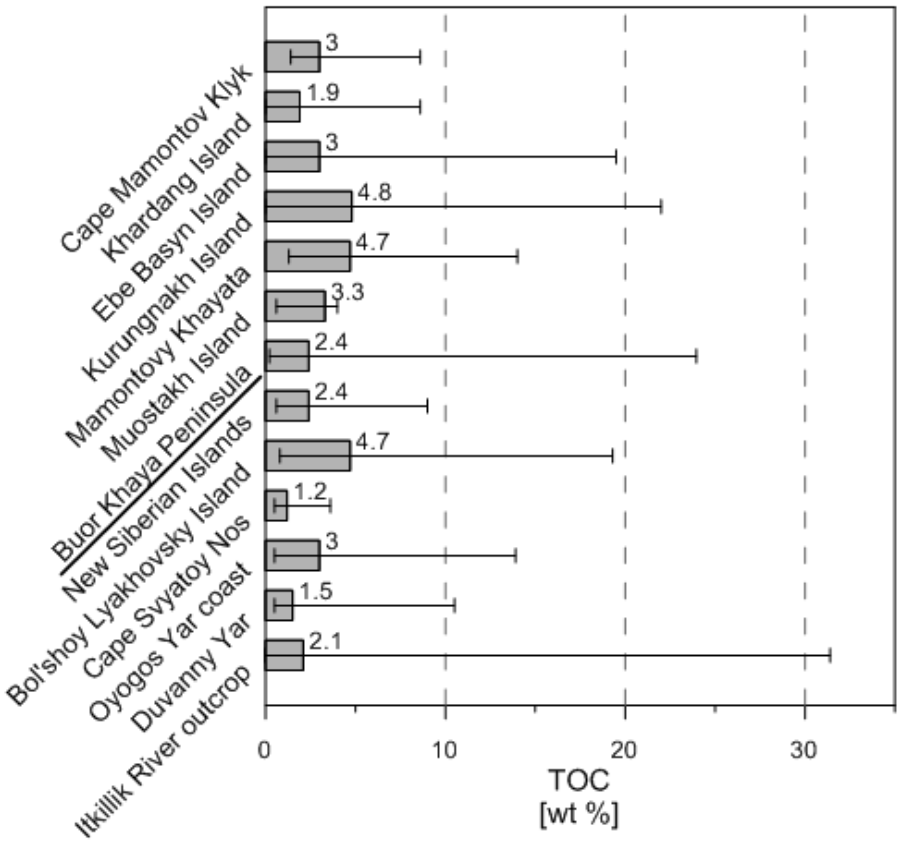

Figure S5. TOC variations from different Yedoma studies sorted from easternmost (Itkillik River, Alaskan North Slope) to westernmost (Mamontov Klyk, western Laptev Sea) studies (Schirrmeister et al., 2008a; Schirrmeister et al., 2008b; Schirrmeister et al., 2011; Strauss et al., 2013), including the present study from Buor Khaya Peninsula. The means are illustrated by the values; the range is shown by the bars.

S3 Supplementary table

Table S1. Statistical significance of the degradation parameters. The null hypothesis of the Mann-Whitney-Wilcoxon and Kruskal–Wallis test is that the mean ranks of the groups are the same, which could is negated if the p-value is <0.05.

Yedoma vs. thermokarst	**TOC**	**CN**	**$\delta^{13}C$**	**CPI**	**HPFA**	**Hopene**
Mann-Whitney-Wilcoxon test, p-value	0.0179	0.0068	0.0010	0.0202	0.0235	0.1161
Profile Buo- 01 vs. 02 vs. 03 vs. 04 vs. 05						
Kruskal-Wallis test, p-value	0.2783	0.0349	0.0127	0.2527	0.0241	0.3518

Supplementary References

Blott, S. J., and Pye, K.: Gradistat: A grain size distribution and statistics package for the analysis of unconsolidated sediments, Earth Surface Processes and Landforms, 26, 1237-1248, doi:10.1002/esp.261, 2001.

Folk, R. L., and Ward, W. C.: Brazos River bar: A study in the significance of grain size parameters, Journal of Sedimentary Petrology, 27, 3-26, 1957.

Goslar, T., Czernik, J., and Goslar, E.: Low-energy 14c ams in poznań radiocarbon laboratory, poland, Nuclear Instruments and Methods in Physics Research Section B: Beam Interactions with Materials and Atoms, 223–224, 5-11, doi:10.1016/j.nimb.2004.04.005, 2004.

Killops, S. D., and Killops, V. J.: Introduction to organic geochemistry, John Wiley & Sons, 2009.

Schirrmeister, L., Grosse, G., Kunitsky, V., Magens, D., Meyer, H., Dereviagin, A., Kuznetsova, T., Andreev, A., Babiy, O., Kienast, F., Grigoriev, M., Overduin, P. P., and Preusser, F.: Periglacial landscape evolution and environmental changes of arctic lowland areas for the last 60 000 years (western laptev sea coast, cape mamontov klyk), Polar Research, 27, 249-272, doi:10.1111/j.1751-8369.2008.00067.x, 2008a.

Schirrmeister, L., Grosse, G., Wetterich, S., Overduin, P. P., Strauss, J., Schuur, E. A. G., and Hubberten, H.-W.: Fossil organic matter characteristics in permafrost deposits of the northeast siberian arctic, Journal of Geophysical Research, 116, G00M02, doi:10.1029/2011jg001647, 2011.

Schirrmeister, L., Kunitsky, V. V., Grosse, G., Kuznetsova, T. V., Derevyagin, A. Y., Wetterich, S., and Siegert, C.: The yedoma suite of the northeastern siberian shelf region: Characteristics and concept of formation, Proceedings of the Ninth International Conference on Permafrost, 2, 1595-1601, 2008b.

Strauss, J., Schirrmeister, L., Grosse, G., Wetterich, S., Ulrich, M., Herzschuh, U., and Hubberten, H.-W.: The deep permafrost carbon pool of the yedoma region in siberia and alaska, Geophys. Res. Lett., 40, 6165–6170, doi:10.1002/2013GL058088, 2013.